NPS-MAE-09-002

NAVAL POSTGRADUATE SCHOOL

MONTEREY, CALIFORNIA

A STUDY ON FRAGILITY ASSESSMENT FOR EQUIPMENT IN A SHOCK ENVIRONMENT

by

Beomsoo Lim
Jarema M. Didoszak

December 2009

Approved for public release; distribution is unlimited

NAVAL POSTGRADUATE SCHOOL
Monterey, California 93943-5000

Daniel T. Oliver
President

Leonard A. Ferrari
Executive Vice President and Provost

This report was prepared by and funded by the Naval Postgraduate School, Monterey, CA 93943.

This report was prepared by:

Beomsoo Lim
Visiting Professor of
Mechanical & Astronautical Engineering

Jarema M. Didoszak
Research Assistant Professor

Reviewed by:

Knox T. Millsaps
Department of Mechanical &
Astronautical Engineering

Released by:

Karl van Bibber
Vice President and
Dean of Research

REPORT DOCUMENTATION PAGE

Form Approved
OMB No. 0704-0188

1. REPORT DATE *(DD-MM-YYYY)*	**2. REPORT TYPE**	**3. DATES COVERED** *(From - To)*
20-12-2009	Technical	Dec 2008 – Dec 2009

4. TITLE AND SUBTITLE
A Study on Fragile Assessment for Equipment in a Shock Environment

5a. CONTRACT NUMBER

5b. GRANT NUMBER

5c. PROGRAM ELEMENT NUMBER

6. AUTHOR(S)
Lim, Beomsoo
Didoszak, Jerema M.

5d. PROJECT NUMBER

5e. TASK NUMBER

5f. WORK UNIT NUMBER

7. PERFORMING ORGANIZATION NAME(S) AND ADDRESS(ES)
Naval Postgraduate School
Monterey, CA 93943-5000

8. PERFORMING ORGANIZATION REPORT NUMBER
NPS-MAE-09-002

9. SPONSORING / MONITORING AGENCY NAME(S) AND ADDRESS(ES)
N/A

10. SPONSOR/MONITOR'S ACRONYM(S)

11. SPONSOR/MONITOR'S REPORT NUMBER(S)

12. DISTRIBUTION / AVAILABILITY STATEMENT
Approved for public release; distribution is unlimited

13. SUPPLEMENTARY NOTES
The views expressed in this report are those of the authors and do not reflect the official policy or position of the Department of Defense or the U.S. Government.

14. ABSTRACT
In this report, the Damage Boundary Theory and related analysis using the Shock Response Spectrum have been investigated. In particular, physics-based computer modeling and simulation using the MSC/NASTRAN code has been performed for the case of a rotational drop test model. Application of the Damage Boundary Theory and subsequent analysis using the Shock Response Spectrum is useful in understanding the isolation level of packaging systems. The results of the computer simulations show the effects of the flexibility in the equipment and nonlinearity of the shock mounts analyzed in this research. The data from these simulations have been compared with the shock test specification, MIL-STD-810.

15. SUBJECT TERMS
Shock, Fragility, Damage Boundary, Shock Response Spectrum, Modeling and Simulation

16. SECURITY CLASSIFICATION OF:			**17. LIMITATION OF ABSTRACT**	**18. NUMBER OF PAGES**	**19a. NAME OF RESPONSIBLE PERSON**
a. REPORT	**b. ABSTRACT**	**c. THIS PAGE**			Didoszak, Jerema
U	U	U	SAR	62	**19b. TELEPHONE NUMBER** *(include area code)* (831)656-2604

Standard Form 298 (Rev. 8-98)
Prescribed by ANSI Std. Z39.18

THIS PAGE INTENTIONALLY LEFT BLANK

ABSTRACT

In this report, the Damage Boundary Theory and related analysis using the Shock Response Spectrum have been investigated. In particular, physics-based computer modeling and simulation using the MSC/NASTRAN code has been performed for the case of a rotational drop test model. Application of the Damage Boundary Theory and subsequent analysis using the Shock Response Spectrum is useful in understanding the isolation level of packaging systems. The results of the computer simulations show the effects of the flexibility in the equipment and nonlinearity of the shock mounts analyzed in this research. The data from these simulations have been compared with the shock test specification, MIL-STD-810.

THIS PAGE INTENTIONALLY LEFT BLANK

TABLE OF CONTENTS

THIS PAGE INTENTIONALLY LEFT BLANK

LIST OF FIGURES

LIST OF TABLES

THIS PAGE INTENTIONALLY LEFT BLANK

I. INTRODUCTION

The reliability of complicated electronic equipment, requiring a high amount of accuracy, depends on the environment in which it is operated. The shock environment is a critical element that affects survivability of these types of equipment. As such, it is important to clearly identify the limitation of shock endurance definitely and provide proper isolation so as not to allow the equipment to exceed the shock endurance range. There are two separate kinds of requirements to consider in solving the shock problem. It is necessary to first establish the shock fragility of equipment and then to design the shock isolation system to mitigate the shock environmental condition which the equipment will experience.

Since R. D. Mindlin announced "Dynamics of Package Cushioning" in 1945, many studies have been made describing the phenomenon of shock and the corresponding shock response. In order to establish a method as an indicator of mechanical shock severity, Shock Response Spectrum (SRS) analysis was developed in the early 1960's by the U.S Department of Defense engineering contractors and government Research & Development facilities. [Ref. 1, 2]

SRS is the response curve which gives the peak response value at any frequencies that a shock would cause a Single Degree of Freedom (SDOF) to respond. SRS analysis is also used to define the environmental condition of equipment [Ref. 3]. From SRS analysis, Pseudo Velocity (PV), which is the relative displacement multiplied by the frequency, is primarily obtained and plotted on Four Coordinate Paper (4CP). The resulting plot is called a Pseudo Velocity Shock Response Spectrum (PVSRS). PVSRS can be used to estimate the damage potential of a shock to a SDOF system.

A simplification of the SRS analysis combined with availability of repeatable shock machines has resulted in the Damage Boundary theory [Ref. 4]. This method was developed in the late 1960's by R. Newton at the Naval Postgraduate School in Monterey, CA.

The fragility of equipment is another characteristic unique to the system or equipment just like size, weight and color. The equipment fragility is determined by using calibrated inputs and measuring a product's response to those specific inputs. This measurement takes the form of a Damage Boundary Curve for shock. This graph defines an area bounded by peak acceleration on the vertical axis and velocity change on the horizontal axis. Any shock pulse experienced by the equipment which can be plotted inside this boundary will cause damage to the equipment whether or not it is packaged.

This report examines the shock response spectrum theory and Damage Boundary theory to better understand the fragility of equipment. Using the finite element method, rotational drop simulations of packaging system have been accomplished for various stiffness cases of a representative piece of equipment. PVSRS of the equipment were obtained at the critical points and the corresponding damage potential was estimated by comparing them to the shock test standard, MIL-STD-810G [Ref. 5].

II. SHOCK RESPONSE SPECTRUM

A. INTRODUCTION

Shock is defined as a non-periodic acceleration or deceleration due to collision, drop, earthquake or explosion. The word “shock” implies a degree of suddenness and severity. Most equipment in weapon systems is exposed to a shock environment during its packaging, handling, shipping and transportation.

Shock Response Spectrum is the curve of maximum response as a function of natural frequency of the responding system. A pulse is a particular form of shock motion. Each shock motion has a characteristic shock spectrum. A shock motion has a characteristic effective value of time duration which need not be defined specifically. Instead, the spectra are made to apply explicitly to a given shock motion by using the natural frequency as a dimensional parameter on the abscissa. Thus the maximum response can be anticipated from the shock spectrum curve easily, if the frequency characteristic of system is given.

In more recent times, even though computer and signal processing technology has made it possible to directly compute the response of specific structures under transient loading, the SRS analysis method continues to be used to assess the shock fragility because of its simplicity and effectiveness [Ref. 2].

B. CONCEPT OF SHOCK RESPONSE SPECTRA

SRS represents the maximum responses of every conceivable SDOF (Single Degree Of Freedom) system mounted base structure, when the base structure is excited by a shock pulse.

Imagine a platform with 1000 different SDOF components mounted on it as shown in Figure 1. Each component has a different resonance frequency, so that every resonance frequency of possible interest is represented. We have the equivalent of such a system when applying the SRS method. We enforce on that platform the acceleration transient that was present on our base frame. Each of the SDOF components will respond

with its own unique acceleration transient. The peak response acceleration level is then computed for each SDOF component. The set of all peak levels is seen to be representative of the severity of the base frame shock transient. This set of peak levels can be collected together to form a spectrum across the frequency range of interest. This is the SRS [Ref. 2].

In Figure 2, the X axis represents Time, the Y axis represents Acceleration and the Z axis represents Frequency. If the time histories for the every frequency of SDOF are plotted in the X-Y plane and the maximum response in each frequency is plotted in the Z-Y plane, then the plot of the Z-Y plane is the SRS.

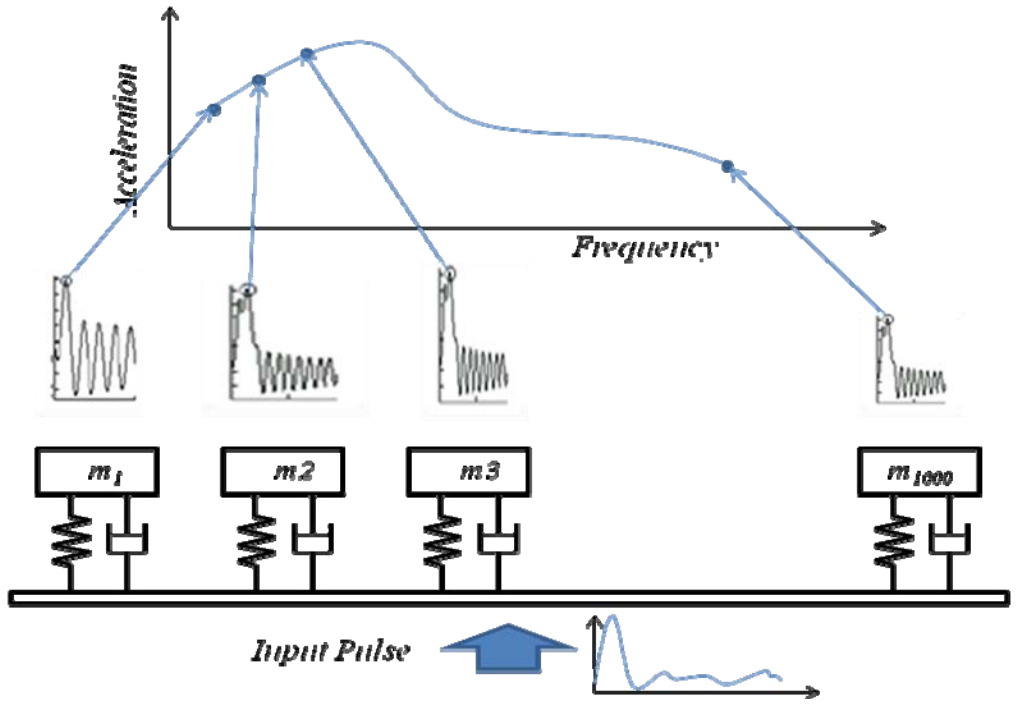

Figure 1. The Concept of Shock Response Spectrum (SRS)

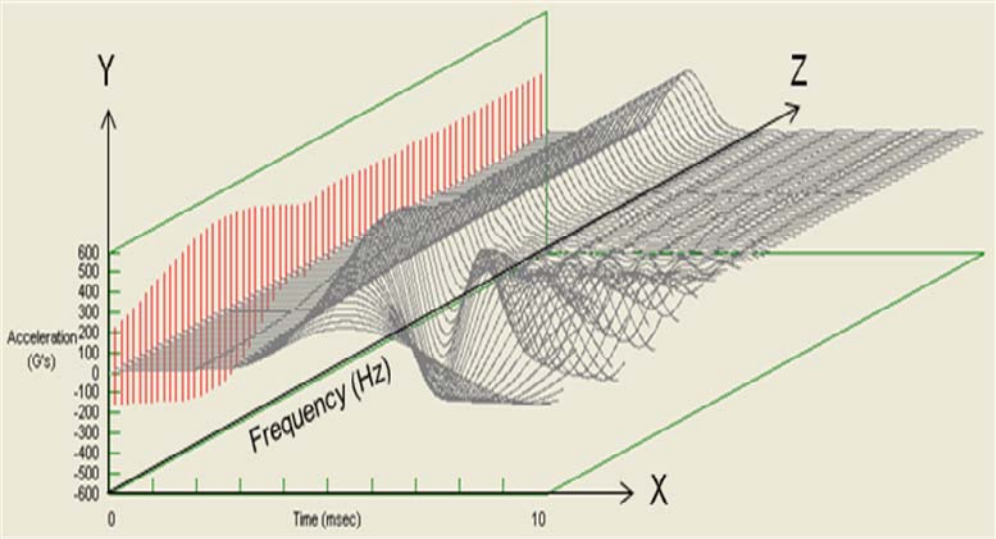

Figure 2. Acquiring the Graph of Shock Response Spectrum

C. CALCULATING SHOCK RESPONSE SPECTRA

The simplest SDOF system is shown in Figure 3. It consists of mass *m* attached by means of spring *k* and damping *c* to a movable base. The mass is constrained to translational motion in the direction *x* axis [Ref. 11].

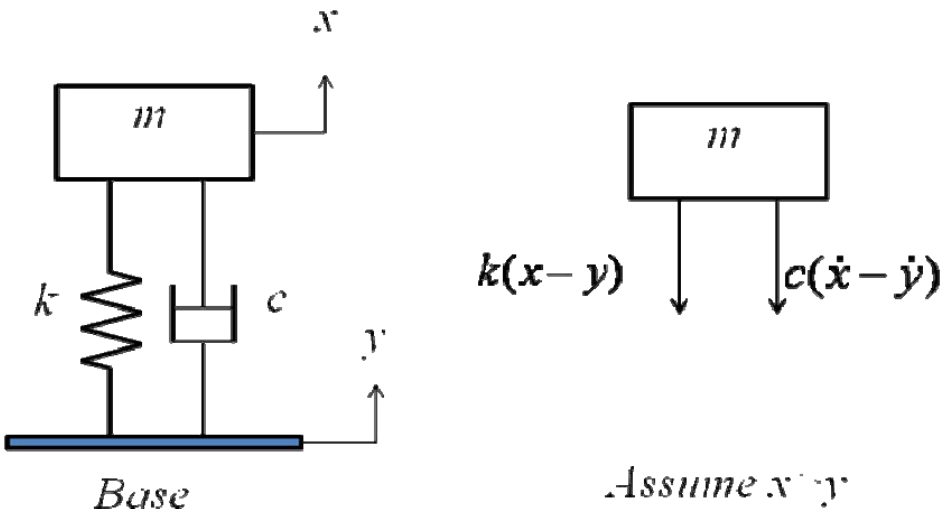

Figure 3. SDOF System with Spring and Damper

The differential equation of motion for the SDOF shown in Figure 3 excited by base motion *y* is as follows:

$$\sum F_x = m\ddot{x} = k(x - y) + c(\dot{x} - \dot{y}) \tag{1}$$

The response motion to be solved in Equation (1) is the relative displacement, z, between the mass response motion, x, and the input displacement, y:

Letting $z = x - y$ and substituting it into Equation (1) gives

$$m(\ddot{z} + \ddot{y}) = -kz - c\dot{z}$$

$$m\ddot{z} + c\dot{z} + kz = -m\ddot{y} \tag{2}$$

Let $\omega_n^2 = \frac{k}{m}$, $\zeta^2 = \frac{C}{C_c}$, $2\zeta\omega_n = \frac{c}{m}$ and substituting those into Equation (2) gives

$$\ddot{z} + 2\zeta\omega_n \dot{z} + \omega_n^2 z = -\ddot{y} \tag{3}$$

Calculation of the differential equation (3) gives the time domain response of relative displacement *z*. The Pseudo Velocity Shock Response Spectrum (PVSRS) value at each frequency is computed by solving for z as a function of time, picking off the maximum value, and then multiplying by ω_n as follows:

$$PV = \omega z \tag{4}$$

Equation (4) shows that pseudo velocity is the relative displacement multiplied by the frequency in radians. Pseudo velocity is not equal to velocity change ΔV , but high PVSRS will indicate what frequencies are seeing the highest $\Delta V's$. PV is also equal to the square root of half the stored energy per unit mass, as shown in Equation (5). This potential energy is equal to the maximum energy stored in the spring of a SDOF system. "U" can also be viewed as the maximum energy that the shock can deliver to a SDOF system at a particular frequency [Ref. 3].

$$PV = \sqrt{\frac{U}{2m}} \tag{5}$$

Equation (5) shows how pseudo velocity can be used to estimate the damage potential of shock to a SDOF system.

Figure 4 and 5 illustrate several shock pulse inputs and their resulting Shock Response Spectra. In Figure 4 and 5, A_p represents the level of the peak acceleration pulse of input, A_c represents the peak acceleration of equipment and f_c represents the natural frequency of equipment. T_e, which is the effective duration of the acceleration pulse, is obtained from the velocity change divided by A_p. For example, $T_e = T$ for the rectangular pulse and $T_e = \frac{2}{\pi} T$ for the half sine wave pulse.

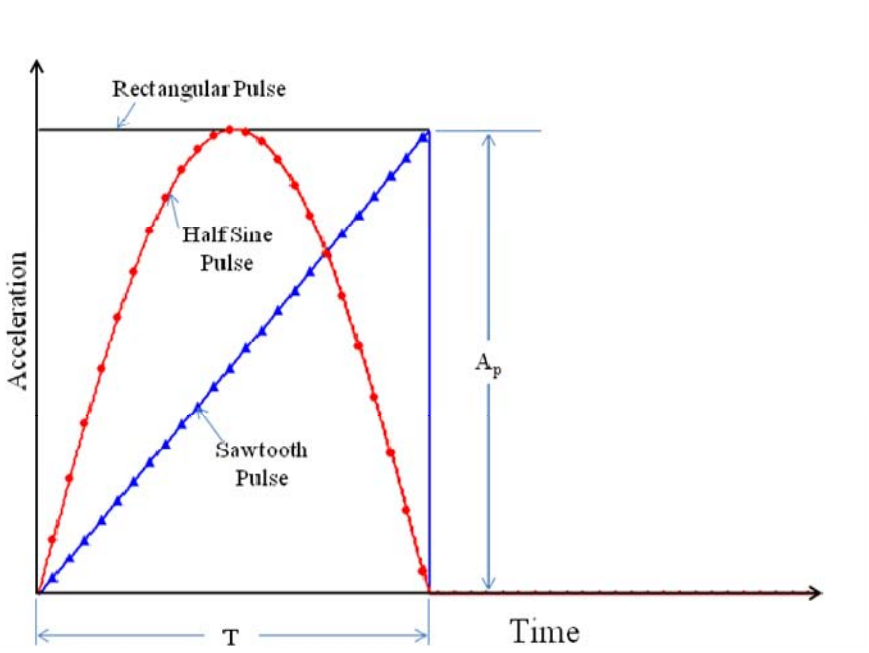

Figure 4. Various Shock Pulse Types

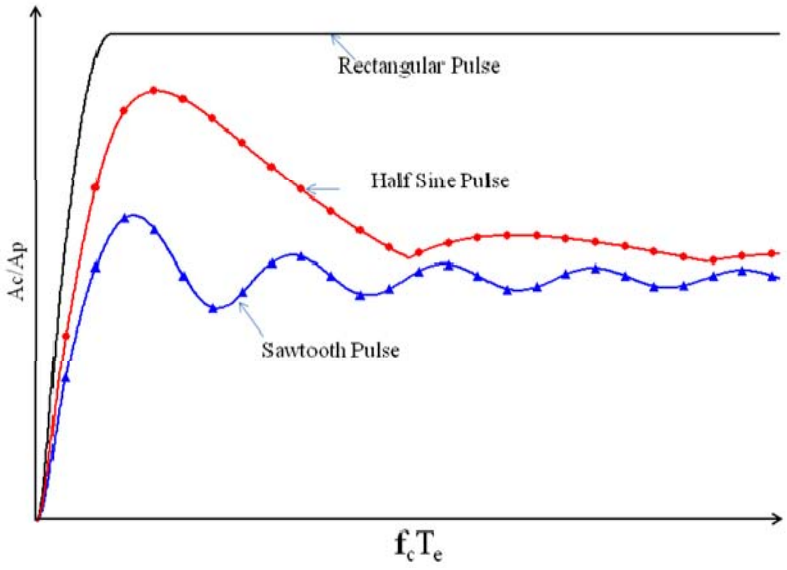

Figure 5. Shock Spectra Resulting from Various Pulses

D. FOUR COORDINATE PAPER (4CP)

Four Coordinate Paper (4CP) is a nomograph of a sine wave, with frequency in Hertz (Hz), deflection in millimeter (mm), pseudo velocity in meters per second (m/sec), acceleration in g's as shown in Figure 6. 4CP is a convenient way of plotting shock response spectra because it illustrates all of the shock motion characteristics on one graph. Figure 6 exhibits the shock response spectrum for a half sine pulse of 10g, 10ms. The figure has four sets of log spaced lines: vertical for frequency, horizontal for pseudo velocity, down and to the right for acceleration, down and to the left for displacement.

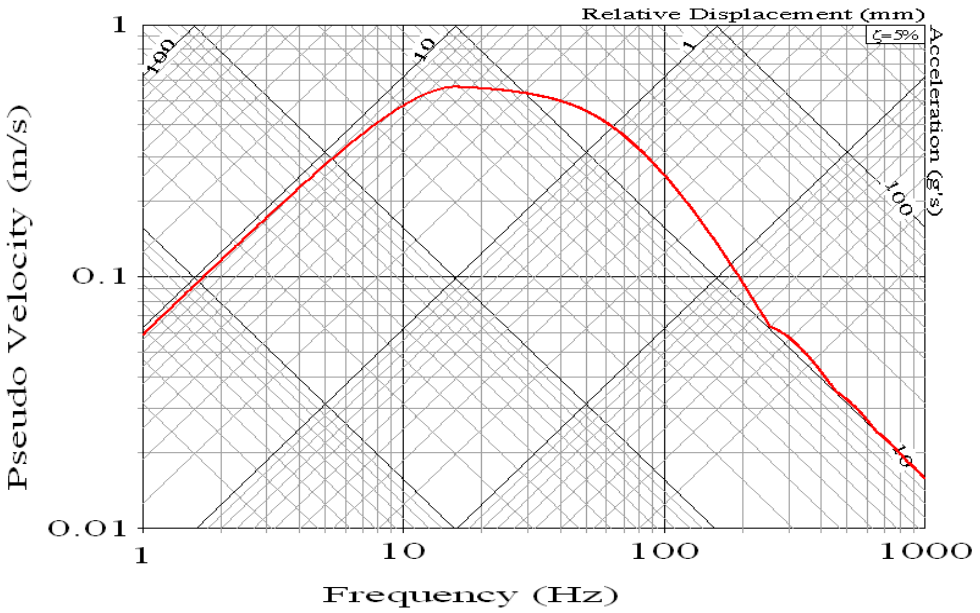

Figure 6. Shock Response Spectrum Curve

III. SHOCK FRAGILITY ASSESSMENT AND TEST PROCEDURE

A. INTRODUCTION

It is important to assess how severe of a shock the equipment can endure in order to provide proper and economic protective package. This is called "Shock Fragility Assessment". Many studies were conducted and test standards developed in order to establish the procedure of shock fragility assessment. Among them, Damage Boundary theory [Ref. 4] and ASTM-D3332 [Ref. 6] are most well-known.

B. DAMAGE BOUNDARY THEORY

The concept of Damage Boundary theory is well-established having been published by Dr. Robert Newton in 1968. The original concept of Damage Boundary was a simplification of Shock Response Spectrum (SRS) where the plot of the damage potential area is bounded by peak acceleration and velocity change. The shock load on the equipment is represented by acceleration level (A_p) and duration time (T) as shown in Figure 7.

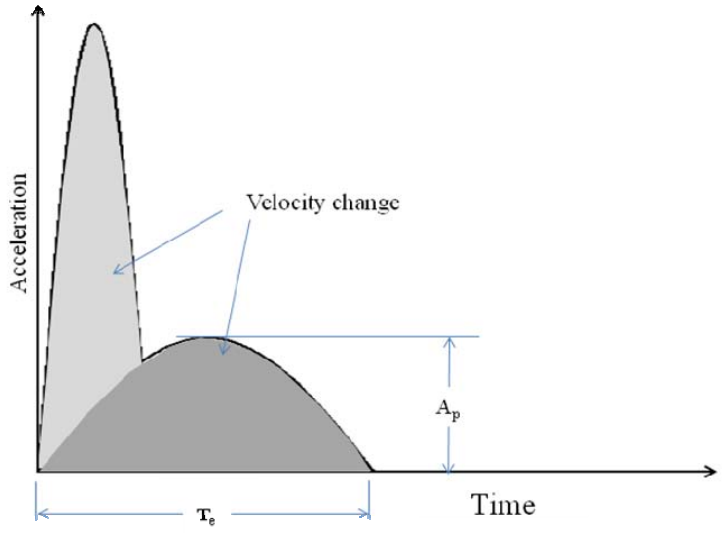

Figure 7. Velocity Change of Shock Pulse

The shaded areas under the time-acceleration curves are velocity change. The velocity change is obtained by Equation (6).

$$V = A_p T_e \tag{6}$$

T_e is the effective duration obtained from real duration time T as was explained in the previous section.

Damage Boundary Curve is obtained from the relationship between peak acceleration and velocity change using Equation (6) and Shock Response Spectrum of various pulses. Consider the shock spectrum for the rectangular pulse shown Figure 8.

In the segments of OA, AB, BC of Figure 8, relationships between the acceleration ratio (A_c/A_p) and frequency ratio (f_c/T_e) of the SRS for the rectangular pulse are as follows:

$$\text{OA}\left(0 \le f_c T_e \le \frac{1}{6}\right) : \frac{A_c}{A_p} = 2\pi f_c T_e \tag{7}$$

$$\text{AB}\left(\frac{1}{6} \le f_c T_e \le \frac{1}{2}\right) : \frac{A_c}{A_p} = 2\sin(\pi f_c T_e) \tag{8}$$

$$\text{BC}\left(\quad f_c T_e \ge \frac{1}{2}\quad\right) : \frac{A_c}{A_p} = 2 \tag{9}$$

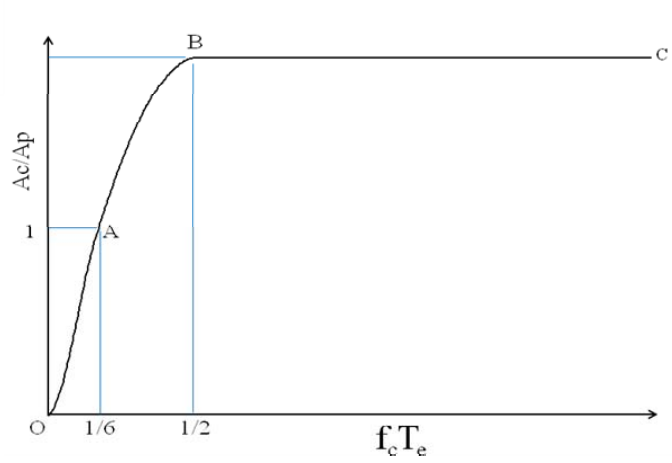

Figure 8. Shock Spectrum of a Rectangular Pulse

Assume that the critical equipment has a specified natural frequency, f_c and the peak acceleration without damage, A_{cs}. In case that effective duration (T_e) of input pulse is short ($f_cT_e \leq \frac{1}{6}$), substituting $A_c = A_{cs}$, $T_e = \frac{V}{A_p}$ in Equation (7) and solving for V gives

$$V = V_i = \frac{1}{2\pi}\frac{A_{cs}}{f_c} \tag{10}$$

Equation (10) represents the maximum velocity change without damage when the excitation frequency of the input pulse is very high compared to the natural frequency of the equipment. Equation (10) indicates that the allowable velocity change is determined by natural frequency and the allowable acceleration of equipment. The acceleration level and duration of input pulse are obtained from Equation (6).

In case that effective duration (T_e) of input pulse is long ($f_cT_e \geq \frac{1}{2}$), substituting $A_c = A_{cs}$ in Equation (9) gives

$$A_p = A_{pr} = \frac{1}{2}A_{cs} \tag{11}$$

Thus Equation (11) represents the maximum acceleration without damage when the excitation frequency of the input pulse is very low compared to the natural frequency

of equipment. Equation (11) then dictates that the allowable acceleration level of shock input is only half of the allowable acceleration of equipment, irrespective of velocity change.

When the frequency ratio of equipment to input shock pulse is between 1/6 and 1/2 $\left(\frac{1}{6} \le f_c T_e \le \frac{1}{2}\right)$, substituting $A_c = A_{cs}$, $T_e = \frac{V}{A_p}$ in Equation (8) gives the relationship between A_p and V as follows;

$$\frac{A_{cs}}{A_p} = 2\ln\left(\pi f_c \frac{\pi f_c V}{A_p}\right) \tag{12}$$

Figure 9 represents Damage Boundary Curve as a function of input acceleration (A_p) and velocity change (V), based upon Equations (10), (11), and (12). The coordinate values of A_p, and V at points A and B are as follow:

Point A : $A_p = A_{cs}, V = V_i$

Point B : $A_p = \frac{1}{2}A_{cs}$ $A_{cs} = 2A_p = 2\frac{V}{T_e}$

$$V = \frac{1}{2}A_{cs}T_e = \frac{1}{4}\frac{A_{cs}}{f_c} = \frac{1}{4}(2\pi V_i) = \frac{\pi}{2}V_i$$

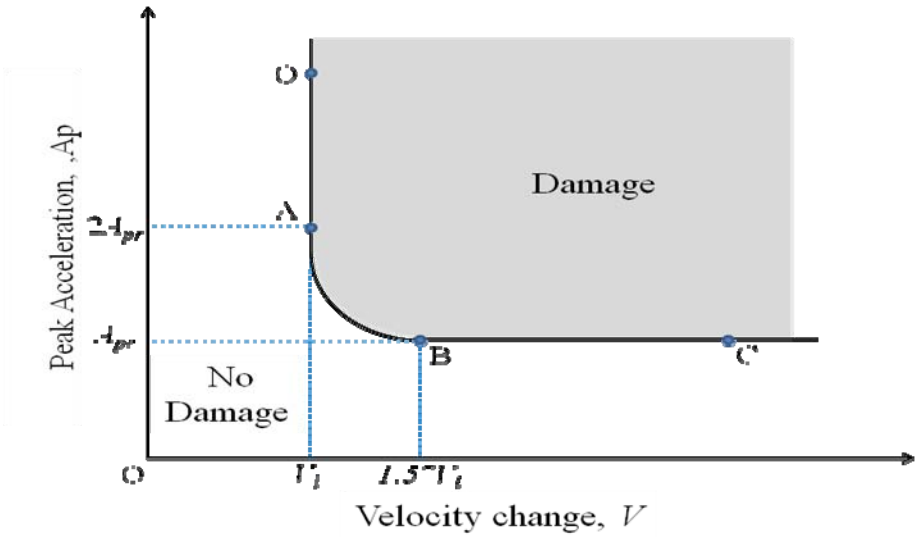

Figure 9. Ideal Damage Boundary Curve

The curve OACD is the border line of damage for the rectangular shock input that has been used here as an example. For shock events in the un-shaded region to the left and below the curve, no equipment damage will result. Conversely, shock events corresponding to points located in the shaded region will cause damage of the equipment.

C. DAMAGE BOUNDARY TEST METHOD (ASTM D3332-99)

In order to design a package system or shipping container for a piece of specific equipment, the shock fragility of that equipment should be first determined. ASTM-D3332-99 provides a test method and procedure to determine the fragility of equipment. When equipment or systems are exposed to a shock environment, the damage of the equipment depends on the velocity change and acceleration. ASTM-D3332-99 defines the procedure to obtain the critical velocity change and critical acceleration at which damage begins using Damage Boundary Curve as was derived in the previous section. Two test methods, the Critical Velocity Change Shock Test, and the Critical Acceleration Shock Test, are outlined here.

1. Test Method A: Critical Velocity Change Shock Test

This test method is used to determine the critical velocity change (V_l) portion of the damage boundary plot for a particular equipment. A shock pulse having any waveform and duration (T_p) between 0.5 and 3ms can be used to perform this test. Since they are relatively easy to control, shock pulses having a half sine shock waveform are normally used. In general, the pulse duration should satisfy the following condition.

$$T_p \leq \frac{167}{f_c}$$

where T_p is maximum shock test machine pulse duration in ms and f_c is the equipment natural frequency in Hz.

To perform this test, initially set the shock test machine so that the shock pulse produced has a velocity change below the anticipated critical velocity change of the equipment. Perform one shock test and examine whether damage due to this shock loading has occurred. Repeat the shock test with incrementally increasing velocity change values until equipment damage occurs. If damage has occurred, the critical velocity change (V_l) is the midpoint between the last successful test and the test that produced failure.

2. Test Method B: Critical Acceleration shock test

This test method is used to determine the critical acceleration (A_{cs}) portion of the damage boundary plot for a particular equipment. Trapezoidal shock pulses are normally used to perform this test. The rise and fall times of 1.8 ms, or less are required in the trapezoidal pulse input because it is not possible to obtain a pulse having infinitely short rise and fall times. Longer rise and fall times cause the pulse form to deviate from the horizontal, introducing errors into the test results.

At first, set the shock test machine so that it will produce a trapezoidal shock pulse having a velocity change of at least 1.57 times as great as the critical velocity change determined in Test Method A. This is done to avoid the rounded intersection of the critical velocity change and critical acceleration lines. Perform one shock test and examine whether damage due to shock has occurred. Repeat the shock test with incrementally increasing acceleration, until equipment damage occurs. If damage has occurred, critical acceleration (A_{cs}) is found to be the midpoint between the last successful test and the test that produced failure. Figure 10 shows an example of the Damage Boundary Test.

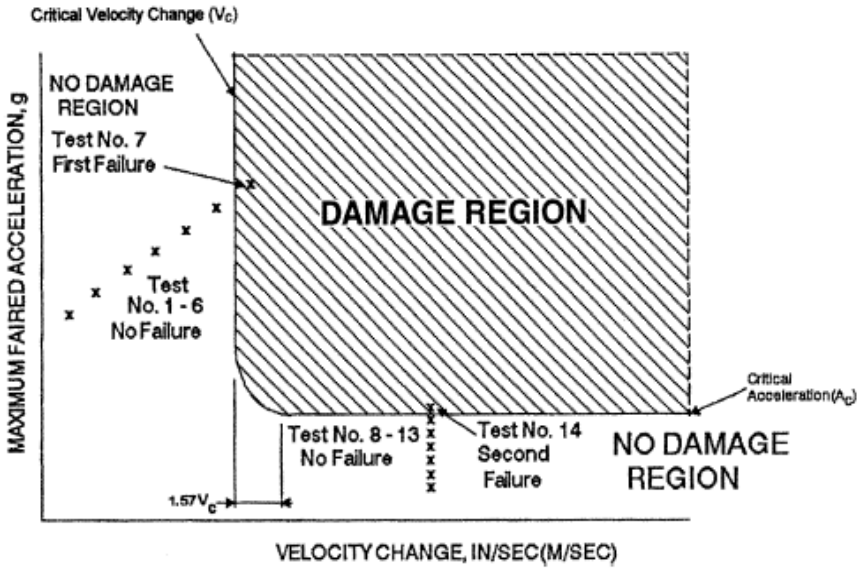

Figure 10. Damage boundary test

Test Method A was performed to determine the critical velocity change. If damage occurs at the 7^{th} test, as indicated in the figure, the midpoint between the 6^{th} and 7^{th} data is defined as critical velocity change. In the second stage of testing, perform Test Method B in order to determine the critical acceleration. If damage occurs at the point of the14^{th} test, as is shown in the figure, the midpoint between 13^{th} and 14^{th} data is defined as critical acceleration.

Test Method A is performed without shock isolator while Test Method B is performed with shock isolator. If no cushioning materials are to be used in the package, the critical acceleration test may be unnecessary. Only the critical velocity change test may suffice in this case.

VI. SIMULATION OF A PACKAGE SYSTEM

Computer simulations were carried out for the drop shock impact of large container to illustrate the application of shock response spectrum analysis. The model was taken from Himelblau and Sheldon's [Ref. 9] chapter on "Vibration of a Resiliently Supported Rigid Body", found in the Shock and Vibration Handbook, 4th Ed. by Harris. It represents a missile container in which a missile is supported by several isolators to protect it from shock impact. The system was subjected to a rotational velocity shock as a result of a drop event where one end of the container was raised to a standardized height. This represents the edgewise drop test in the package test specification.

MSC/PATRAN [Ref. 13] was used in the finite element modeling of this equipment container while MSC/NASTRAN [Ref. 14] was used for conducting the analysis. Normal mode analysis, linear and nonlinear transient analysis were performed for several cases. The analyses were divided into four stages. The first stage was rigid body analysis. The normal mode and linear transient analyses for the rigid body model were conducted and the results were compared with previous research [Ref. 10]. In the second stage, the rigid body model of equipment was replaced by a beam element model using the Finite Element Method. Three kinds of stiffness: low, medium and high, were used to analyze the effects of flexibility of the equipment. The normal mode and linear transient analyses were performed and the results were compared with those of the rigid body analysis of the previous stage. The effects of location of critical component were also investigated. The third stage is a non-linear transient analysis. The nonlinear effects of the isolators were investigated when the equipment was modeled with a medium stiffness. In general, shock mounts using rubber material show a non-linearity in the displacement vs. force curve. In the final stage of this investigation the results were compared with the specifications of shock test as per the MIL-STD-810 and some suggestions are included based upon the results.

Figure 11 shows the 2-dimensional drop test model with symmetry about the YZ plane. This system was subjective to a rotational shock velocity as a result of an edgewise drop. Table 1 shows the dimensions of Figure 11.

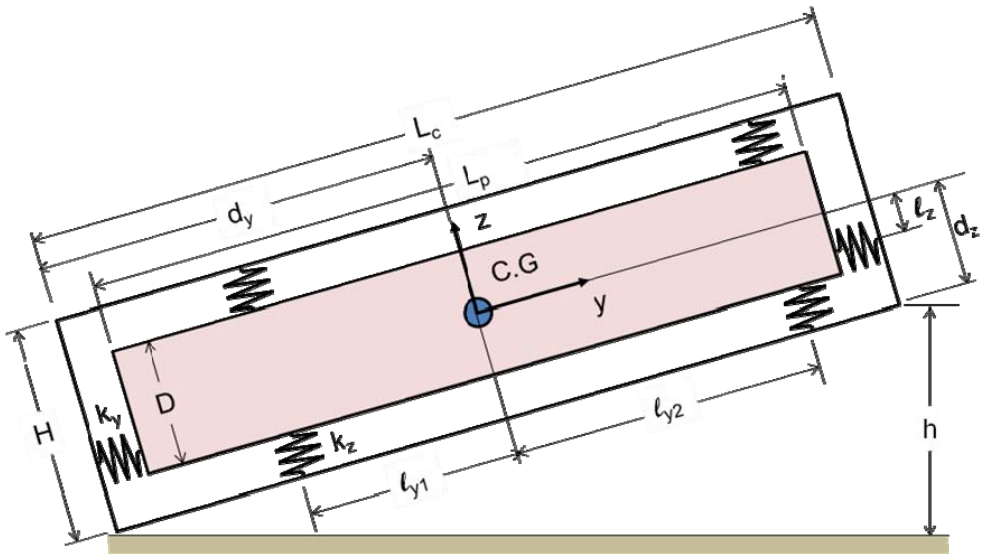

Figure 11. Drop Test Model

Table 1. Dimension of Container and Payload

Item		Unit	Dimension
Container	Length(L_c)	mm	4,267.2
	Width/Height(H)	mm	1,066.8
Payload	Length(L_p)	mm	3,657.6
	Diameter(D)	mm	609.6
	Weight	kg	680.4
	MOI(I_{xx})	kg•mm^2	7.74×10^8
Isolator	Location(l_{y1},l_{y2})	mm	660.4, 1727.2
	Location(l_z)	mm	266.7
	Stiffness_y(k_y)	N/m	8.75×10^4
	Stiffness_z(k_z)	N/m	1.75×10^5

A. RIGID BODY ANALYSIS

1. Model Description

Figure 12 shows rigid body model. The node is placed in the CG (Center of Gravity) point to impose a concentrated mass. The other nodes are placed in connection points with six isolators. The payload is connected to the container box by six spring elements and six damping elements. To connect the node of concentrated mass with the nodes of spring elements and damping elements rigidly, one MPC (Multiple Point Constraint) is used. The 2-dimensional modeling is conducted in YZ plane because the system is symmetric in the YZ plane. Graphic effects are imposed to maintain a square box shape.

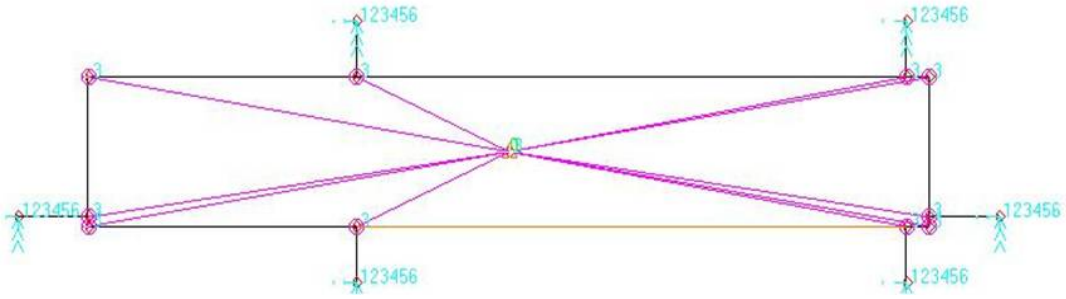

Figure 12. Configuration of the Rigid Body Model

2. Normal Mode Analysis

Table 2 and Figure 13 show the natural frequencies and the mode shapes respectively, for the rigid body model as a result of the normal mode analysis in MSC/NASTRAN. As shown in Figure 13, the first mode represents the translation of the payload in the Y direction, the second mode represents the translational mode in the Z direction and the third mode represents the rotational mode in the X direction.

In Figure 14, the response of the system at the CG is plotted as a function of frequency for the Y and Z directions. This figure shows that the first mode is most dominant in the Y direction and the third mode is most dominant in the Z direction. Comparisons between this study and the reference study [Ref. 10] for natural frequencies are shown in Table 2. These values agree with each other.

Table 2. Natural Frequencies for the Rigid Body Model

Items	1st	2nd	3rd
M.A.Talley	**3.58**	**6.02**	**9.75**
MSC/NASTRAN	3.58	6.03	9.75

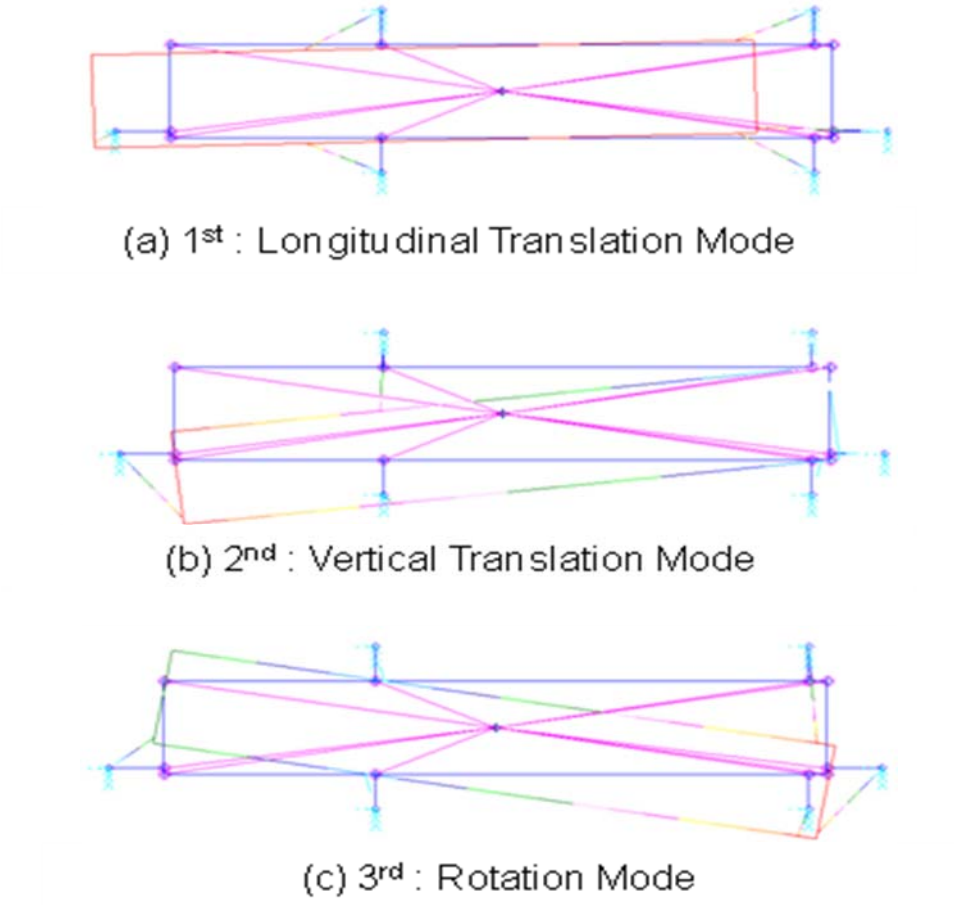

Figure 13. Rigid Body Mode Shapes

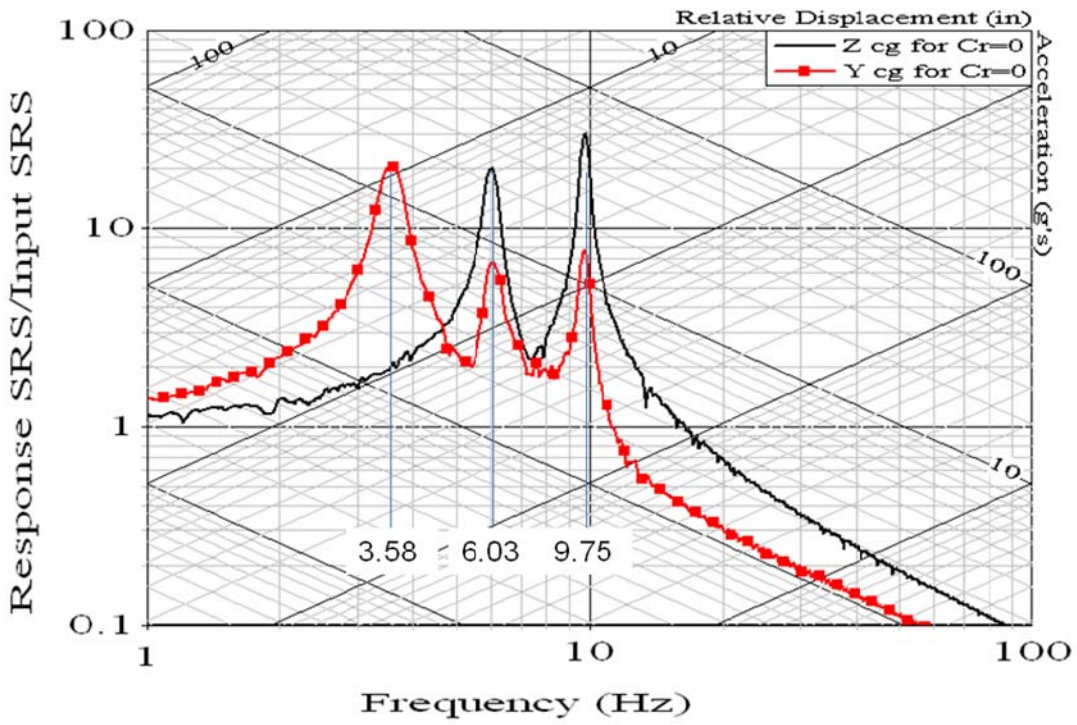

Figure 14. Responses from Rigid Body Analysis

3. Transient Analysis

Linear transient analysis was performed using the MSC/NASTRAN Transient Module. The system was subjective to a rotational shock velocity of 0.38 rad/sec, as a result of a drop event where one end was raised to a height of 36 inches. In the modeling, initial velocities of center of gravity (CG) are calculated and inputted at the moment that the container touches the ground.

Comparisons between the current study and Himelblau's [Ref. 11] along with M. A. Talley's [Ref. 10] calculations for peak acceleration at the center of gravity are shown in Table 3 for the case without damping. There is good agreement with one another. Figures 15 and 16 show the calculated time histories for the Z and Y directions, respectively. Comparing them to the case where 10% damping is applied, the differences in peak acceleration and phasing are observed if damping is ignored. For example, in the Z direction in Figure 5, the peak un-damped acceleration is about 1.2 times greater than the 10% damped acceleration case, which also occurs at a much later time.

Table 3. Peak response comparisons

Response	Himelblau[1]	M. A. Talley	MSC/NASTRAN
Y acceleration at CG	0.74 g's	0.72 g's	0.71 g's
Z acceleration at CG	4.09 g's	4.11 g's	4.11 g's

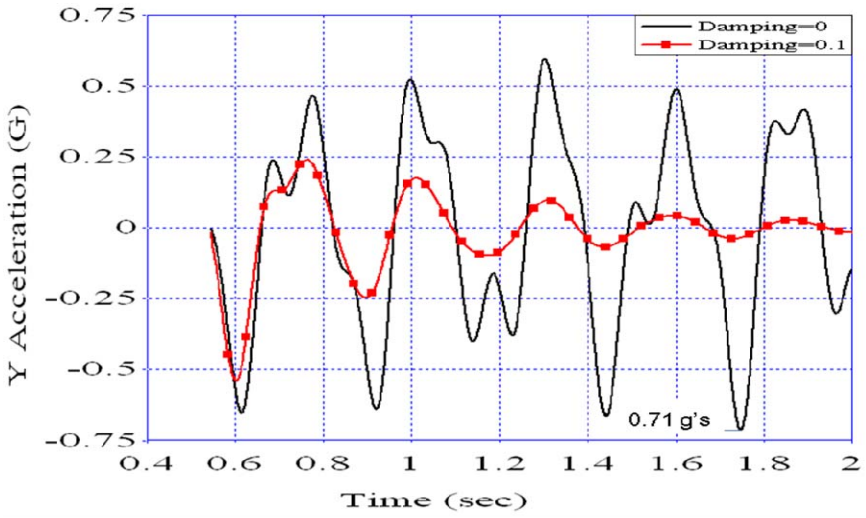

Figure 15. Time Histories for Y Acceleration at the Center of Gravity

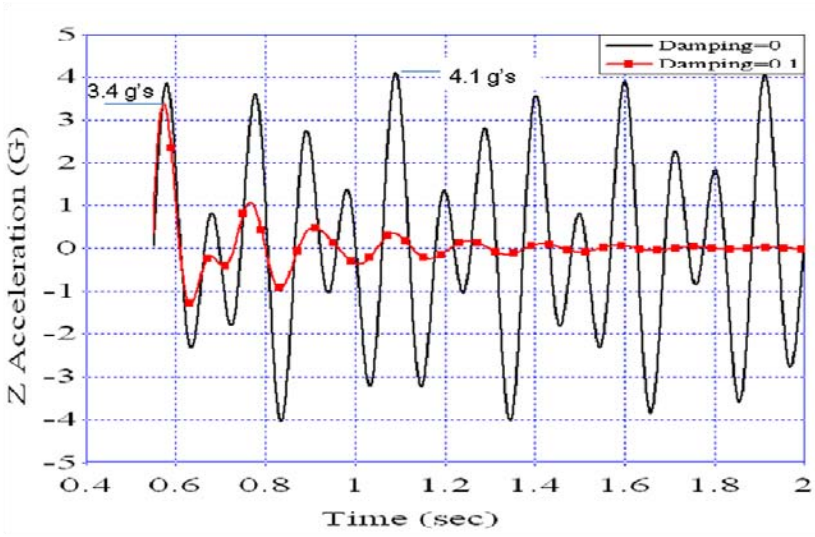

Figure 16. Time Histories for Z Acceleration at the Center of Gravity

B. FLEXIBLE BODY ANALYSIS

1. Model Description

Figure 17 shows the finite element model for the package system. The modeling process was accomplished using the computer code MSC/PATRAN. Beam elements are used to make the model of the representative payload loaded inside of the container. The 2-dimensional modeling is conducted in the YZ plane because the system is symmetric for the YZ plane. 18 beam elements, 6 spring elements and 6 damping elements are used for the model as shown Figure 7. The beam cross section is in the shape of a pipe and the supporting points of the shock mounts are placed in the surface of the payload. Here four MPCs (Multiple Point Constraint) are used to constrain the nodes of the beam elements and supporting points of the mounts.

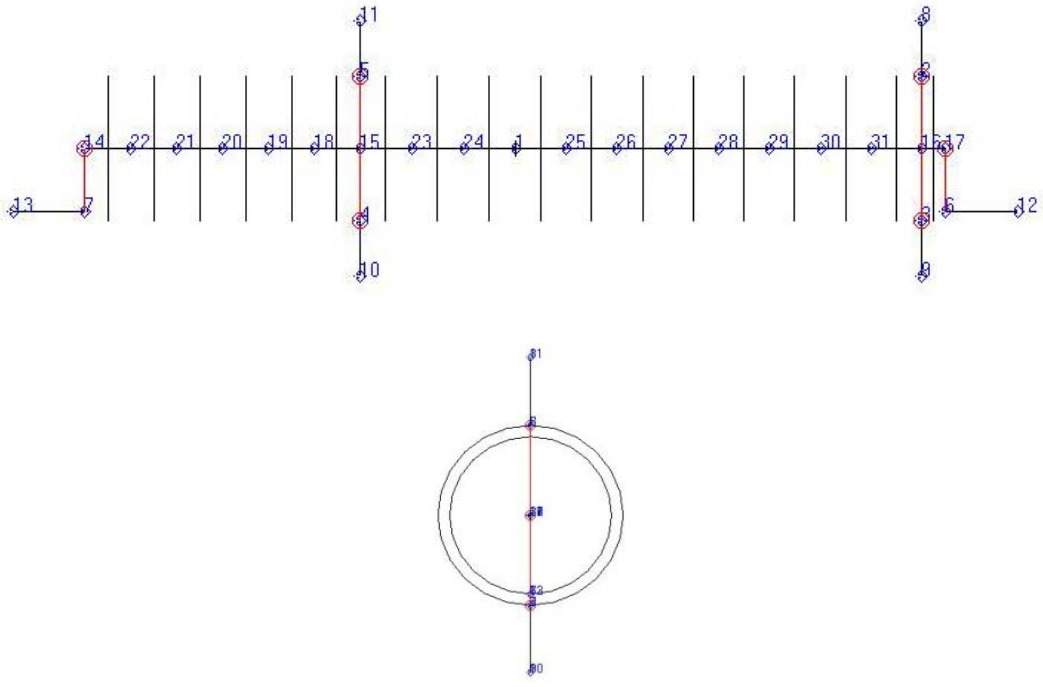

Figure 17. Finite Element Model for the Flexible Body

2. Normal Mode Analysis

The normal modes for the model were solved using MSC/NASTRAN. Table 4 and Figure 18 show the natural frequencies and the mode shapes respectively. As shown in Figure 18, modes 1 through 6 consist of three rigid body modes and three flexible body modes. The first mode represents the translational mode of payload in the Y direction, the second mode represents the translational mode in the Z direction and third mode represents the rotational mode the X direction. The 4^{th} mode indicates the first bending of payload, the 5^{th} mode indicates the second bending of payload and 6^{th} mode exhibits the compression of payload in the longitudinal direction.

Table 4 shows that rigid body modes 1 through 3 became more separated from the bending modes of payload when the stiffness of payload is much higher. In this case, the natural frequency and mode shapes are almost the same as those found in the rigid body model. Conversely, when the stiffness of the payload is low, the bending modes of the payload become close to those of the rigid body modes. In this case, the natural frequencies of the system become low and the mode shapes are so complicated that they are difficult to be differentiated from each other.

Table 4. Model Natural Frequencies

Items		Rigid Body Mode			Flexible Mode		
		1^{st}	2^{nd}	3^{rd}	4^{th}	5^{th}	6^{th}
Rigid Body		3.58	6.03	9.75	-	-	-
Flexible Body	High Stiffness	3.58	6.03	9.74	83.6	189.4	232.0
	Middle Stiffness	3.56	5.94	9.16	28.1	60.7	73.5
	Low Stiffness	3.40	4.92	6.11	13.6	21.9	23.7

1st : Longitudinal Rigid Body Mode

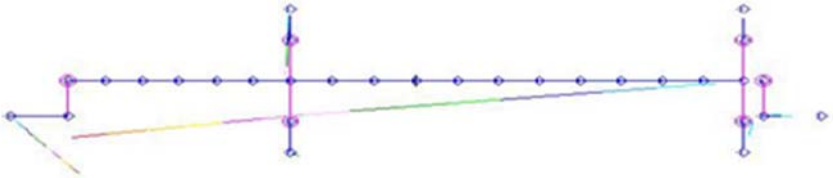

2nd : Vertical Rigid Body Mode

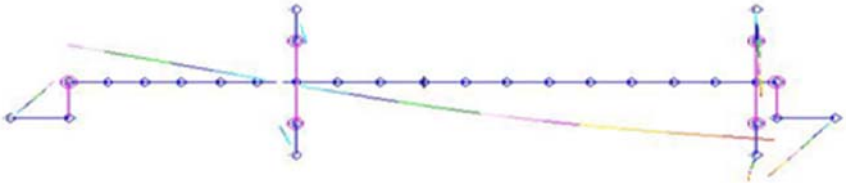

3rd : Rotational Rigid Body Mode

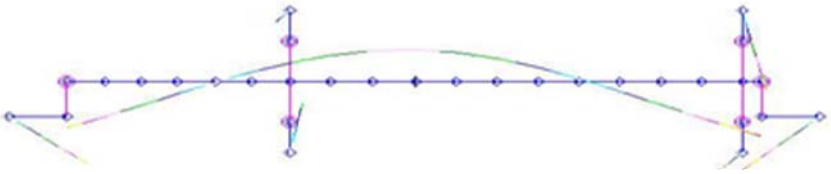

4th : Beam First Bending Mode

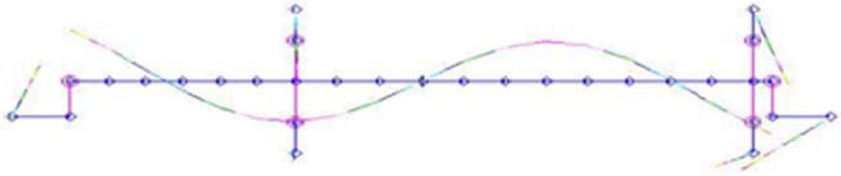

5th : Beam Second Bending Mode

6th : Beam Longitudinal Mode

Figure 18. Mode Shape of the Flexible Body

3. Transient Analysis

A linear transient analysis was performed using MSC/NASTRAN Transient module. The system was subjective to a rotational shock velocity of 0.38 rad/sec, as a result of a drop where one end was raised to a height of 36 inches. In the modeling, initial velocities of each node of beam element is calculated and inputted at the moment that the container touches the ground.

The Young's modulus of the beam elements was changed to investigate the effect of difference of natural frequencies between the rigid body modes and flexible body modes. Three cases, high, medium and low stiffness, are considered. In the high stiffness case, the first bending frequency of the payload, which is 106.6Hz, is much higher than the rigid body frequency, which is 7.22Hz. In this case, the payload responds like a rigid body, so the flexibility of the payload hardly ever affects the response. The medium stiffness was then placed into the model and a value for the first bending frequency of the payload, which is 33.5Hz, about 4 times higher than the rigid body frequency is used. Here flexibility of the payload definitely affects its response. A low stiffness case with a first bending frequency, of 10.7Hz, close to the rigid body frequency was also used. In this case, the responses are very different from those of rigid body model.

The peak accelerations in the center of gravity (CG) are obtained from the time history for each case and then the Shock Response Spectrums (SRS) are calculated. 4CP pseudo velocity curves are used to display the SRS. The damping effects were not considered in the MSC/NASTRAN transient analysis but included as 5% in the calculation of the SRS. Table 5 shows the comparison of peak acceleration for the several cases. It shows that the peak accelerations of center of gravity increase as the stiffness of payload become lower.

Table 5. Peak Response Comparisons

Response	Rigid	High	Medium	Low
Y acceleration at CG	0.74 g's	0.84 g's	1.17 g's	1.2 g's
Z acceleration at CG	4.09 g's	4.59 g's	6.67 g's	8.91 g's

Figures 19 through 30 show the time history and SRS of acceleration at the center of gravity location of the payload. Here the rigid body models for several stiffness cases are compared. They show that the responses are closer to those of rigid body model as the stiffness of payload is higher, and it hardly affects the longitudinal responses.

Figures 19 through 22 compare the high stiffness case of the payload to the rigid body model. These time histories and SRSs are very similar. So, when the difference of the natural frequencies between the rigid body mode and the first bending mode are great, simple rigid body analysis is good enough for accurate results.

Figures 23 through 26 show the time history and SRSs for the medium stiffness case of the payload. In the time history plots there seems to be large differences between the two curves, but the SRS curves show that these differences occur in the high frequency range. In the low frequency range, the rigid body motion is dominant and almost same as rigid body model. In the high frequency range, which is taken to be higher than 20Hz, response of the medium stiffness model is higher than the rigid body model due to the flexible mode of the payload. So in this area, the shock fragility is investigated.

Figures 27 through 30 represent the time history and SRSs for the low stiffness case of the payload. These plots show there is little difference in the longitudinal direction (Y), but the acceleration of vertical direction (Z) is greatly increased. The pseudo velocities are also increased in the bending mode of the payload as well as the rigid body mode cases. This then indicates that when the package system is designed, isolators should be selected not to be close to natural frequency of payload.

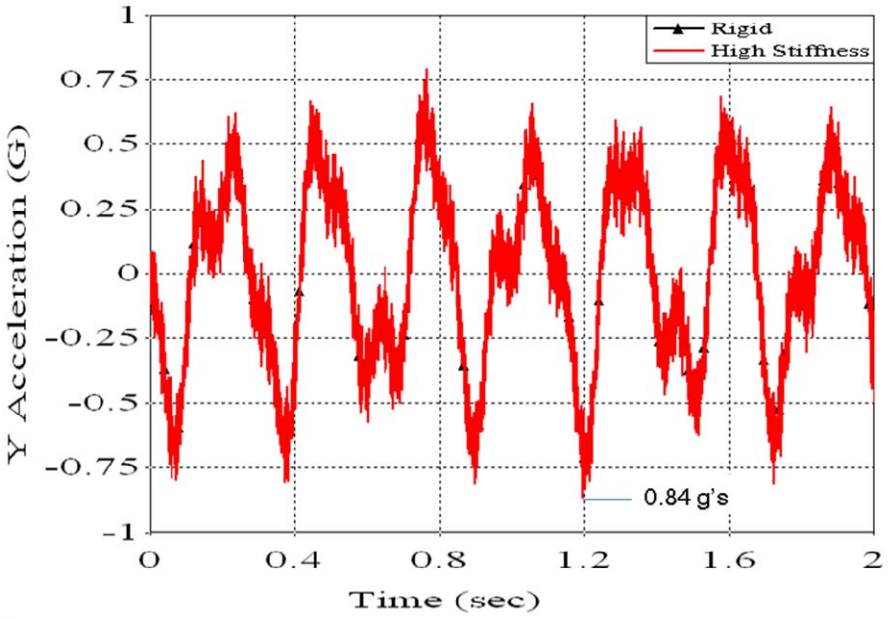

Figure 19. Time Histories for Y Acceleration at the Center of Gravity (High Stiffness Case)

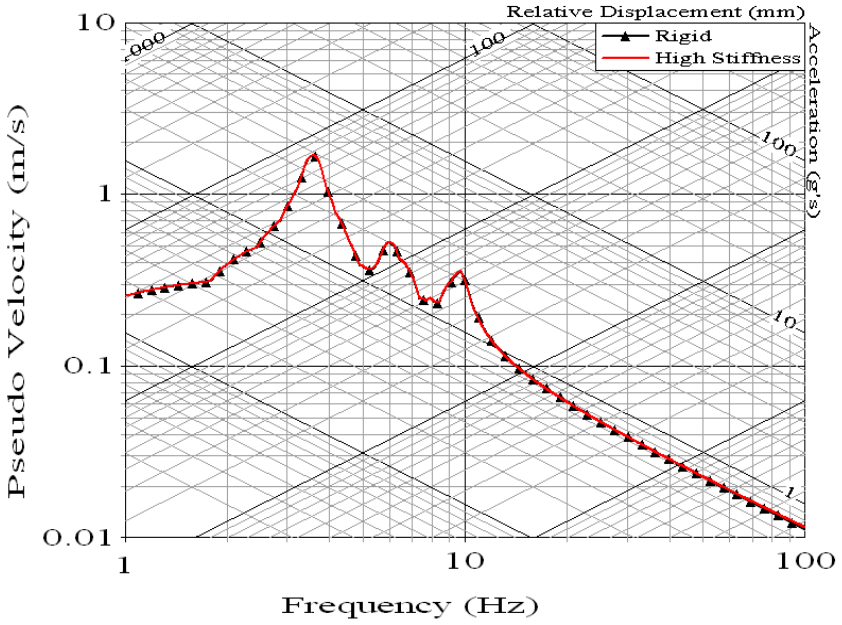

Figure 20. Pseudo Velocity for Y Acceleration at the Center of Gravity (High Stiffness Case)

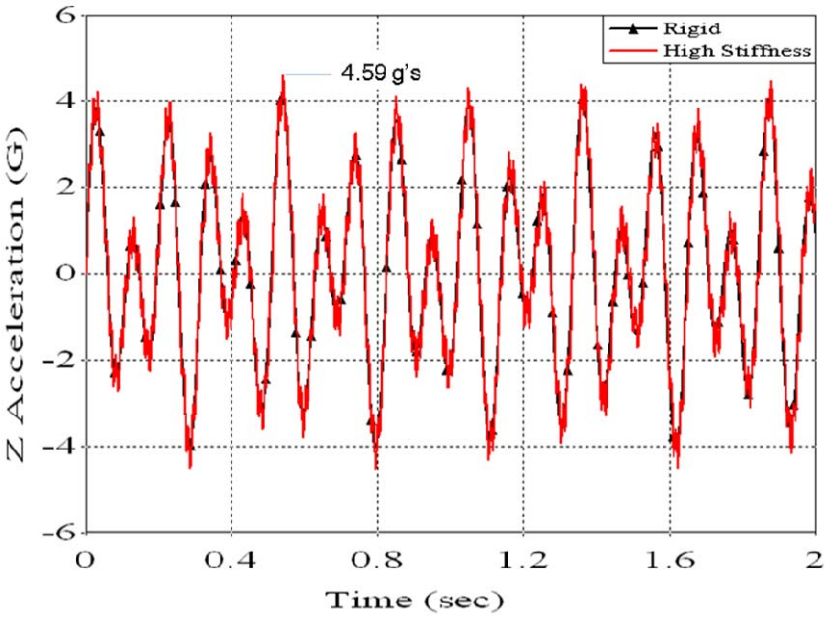

Figure 21. Time Histories for Z Acceleration at the Center of Gravity (High Stiffness Case)

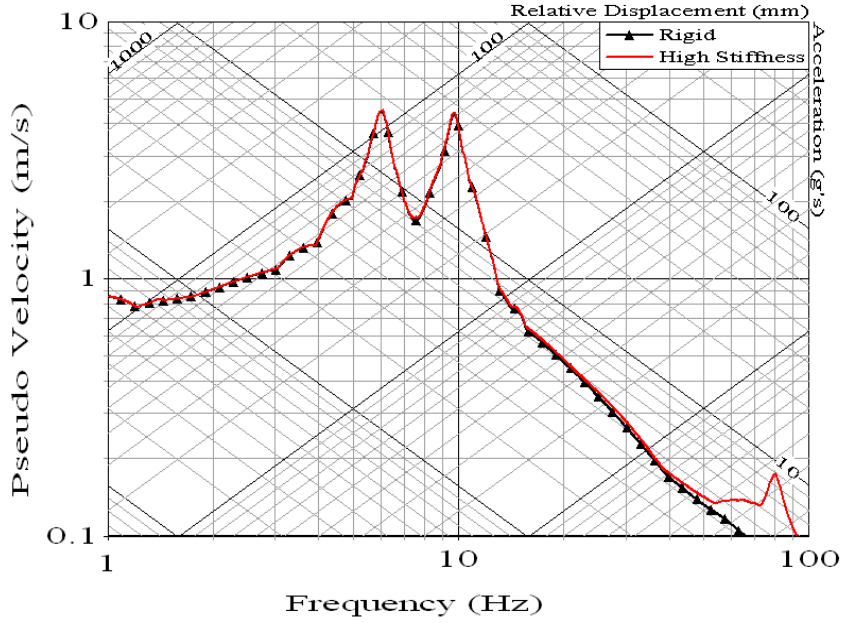

Figure 22. Pseudo Velocity for Z Acceleration at the Center of Gravity (High Stiffness Case)

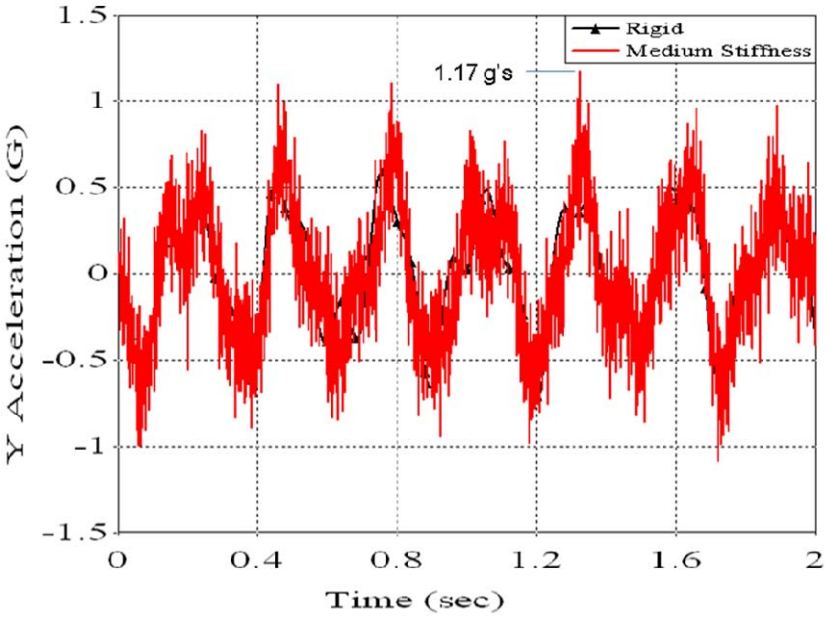

Figure 23. Time Histories for Y Acceleration at the Center of Gravity (Medium Stiffness Case)

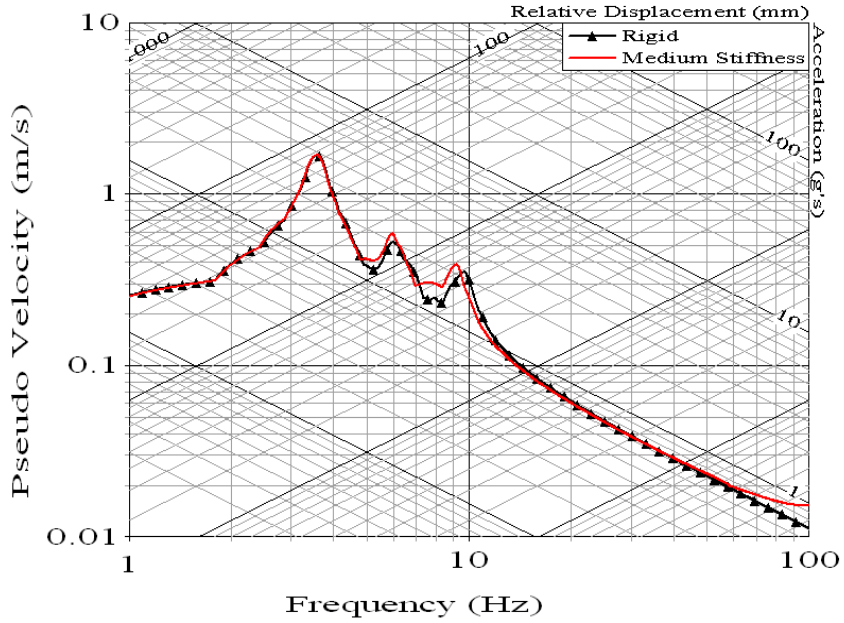

Figure 24. Pseudo Velocity for Y Acceleration at the Center of Gravity (Medium Stiffness Case)

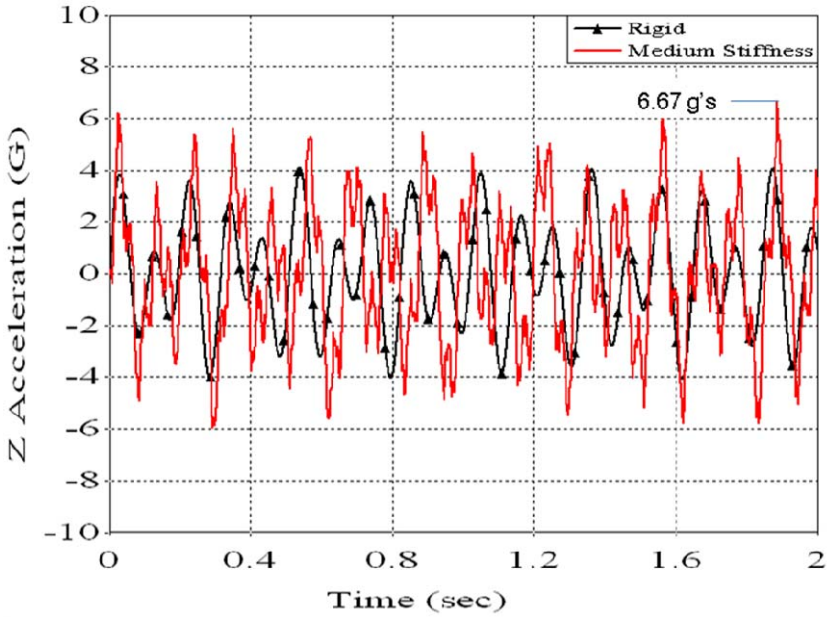

Figure 25. Time Histories for Z Acceleration at the Center of Gravity (Medium Stiffness Case)

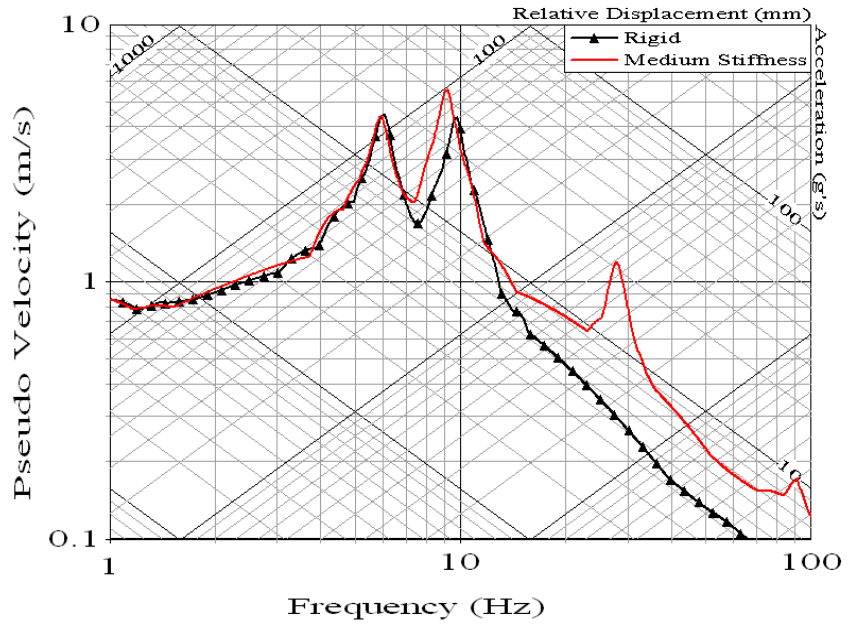

Figure 26. Pseudo Velocity for Z Acceleration at the Center of Gravity (Medium Stiffness Case)

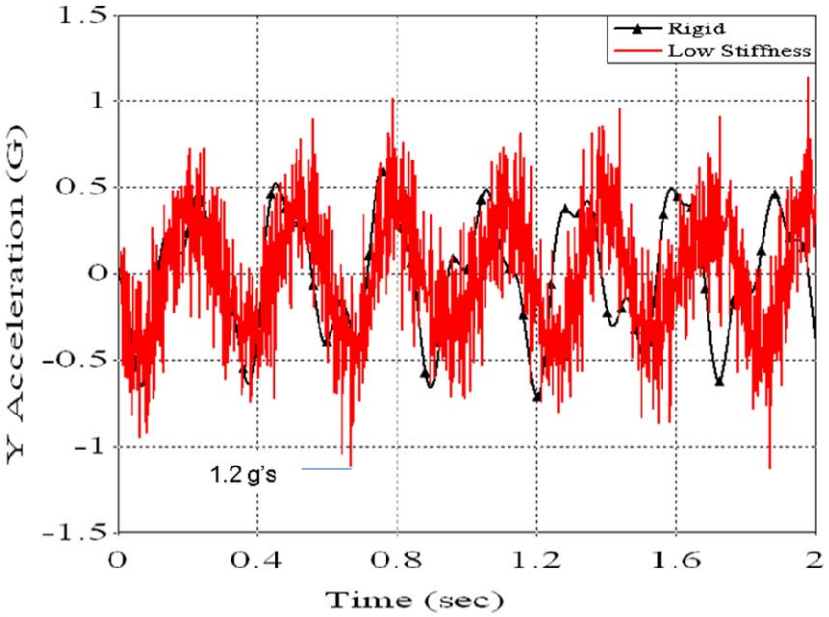

Figure 27. Time Histories for Y Acceleration at the Center of Gravity (Low Stiffness Case)

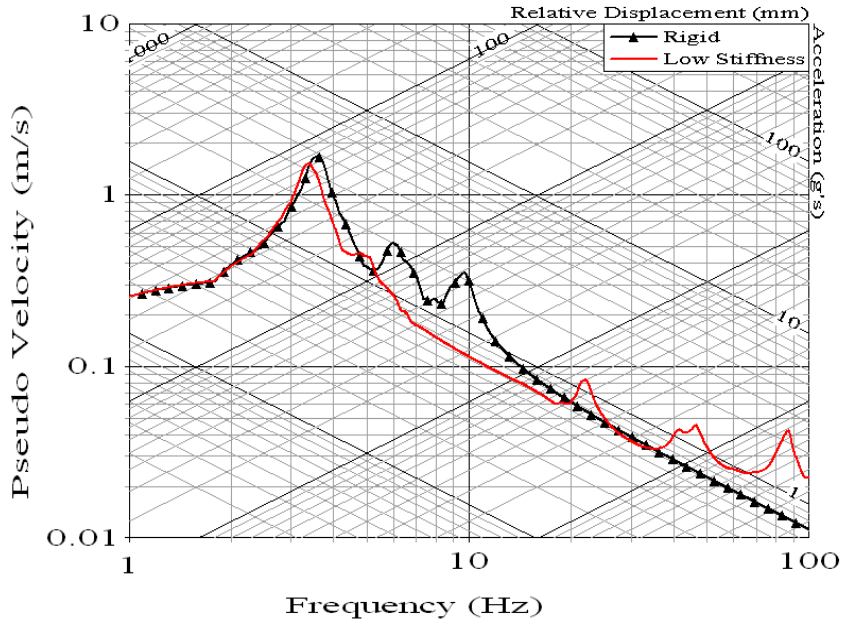

Figure 28**. Pseudo Velocity for Y Acceleration at the Center of Gravity (Low Stiffness Case)**

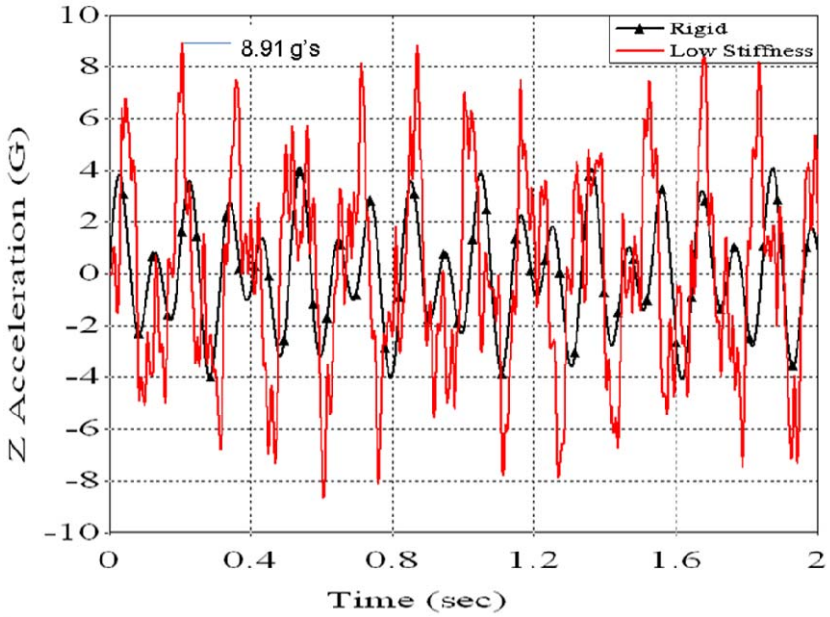

Figure 29. Time Histories for Z Acceleration at the Center of Gravity (Low Stiffness Case)

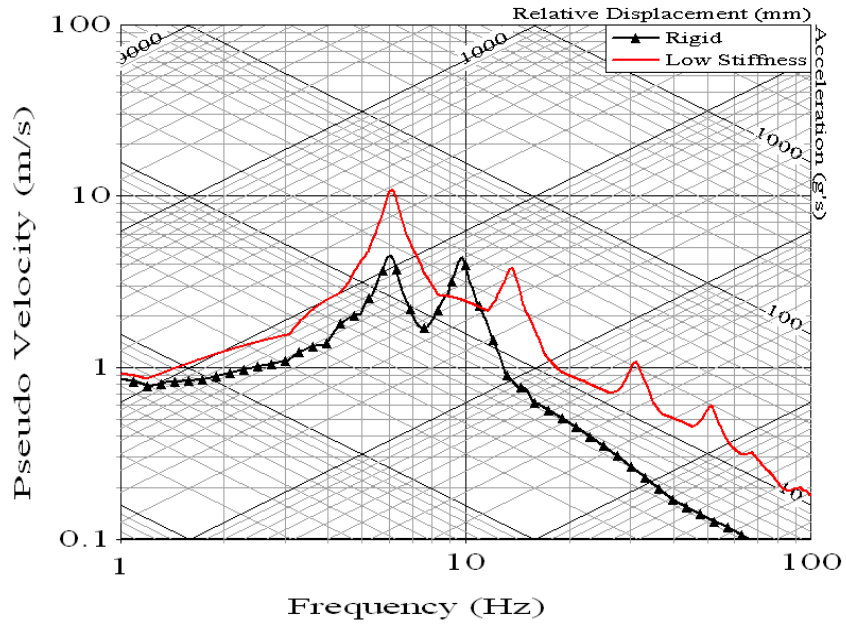

Figure 30. Pseudo Velocity for Z Acceleration at the Center of Gravity (Low Stiffness Case)

Table 6 shows the peak acceleration of several locations of payload. The responses of both ends are higher than that of the center of gravity.

Table 6. Peak Response Comparisons

Response	Left End	CG	Right End
Y acceleration at CG	1.63 g's	1.17g's	2.20 g's
Z acceleration at CG	11.95 g's	6.67 g's	11.78 g's

Figures 31 through 34 compare the time history and SRSs for the various locations of the payload. The SRSs show that there is little difference in the longitudinal direction but the vertical responses are very different from each other. The responses of the left and right ends are higher than those at the center of gravity. So the effects of location of the critical item should be considered when the package system for a long payload such as a missile is designed.

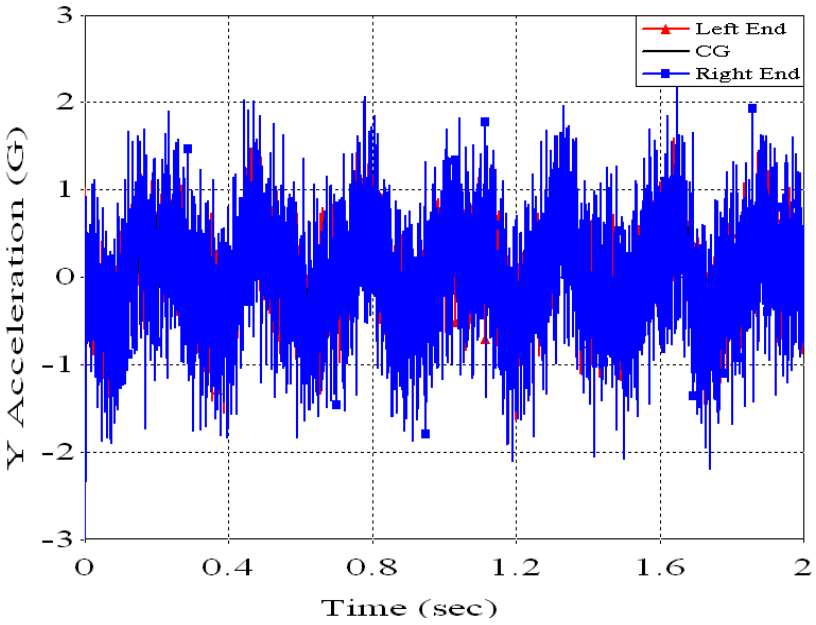

Figure 31. Time Histories for Y Acceleration at Various Locations

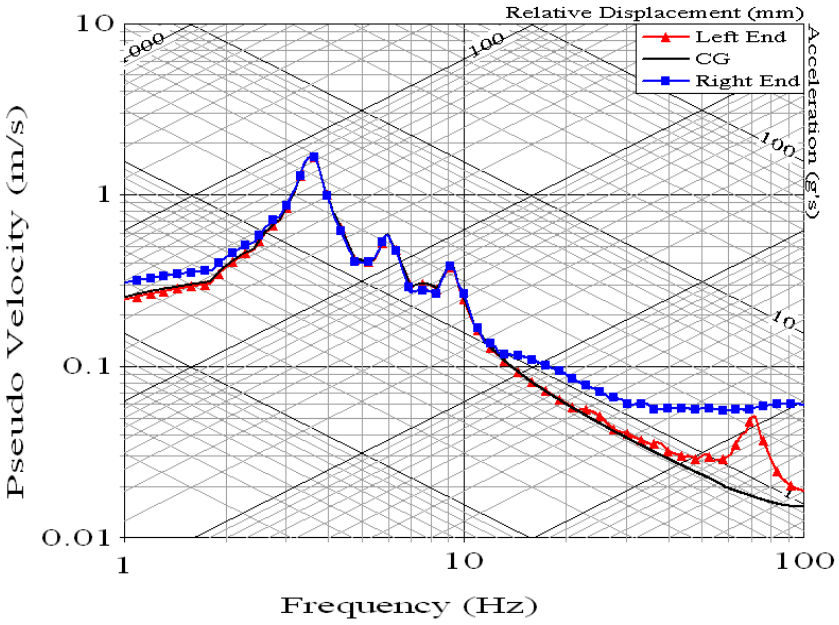

Figure 32. Pseudo Velocity for Y Acceleration at Various Locations

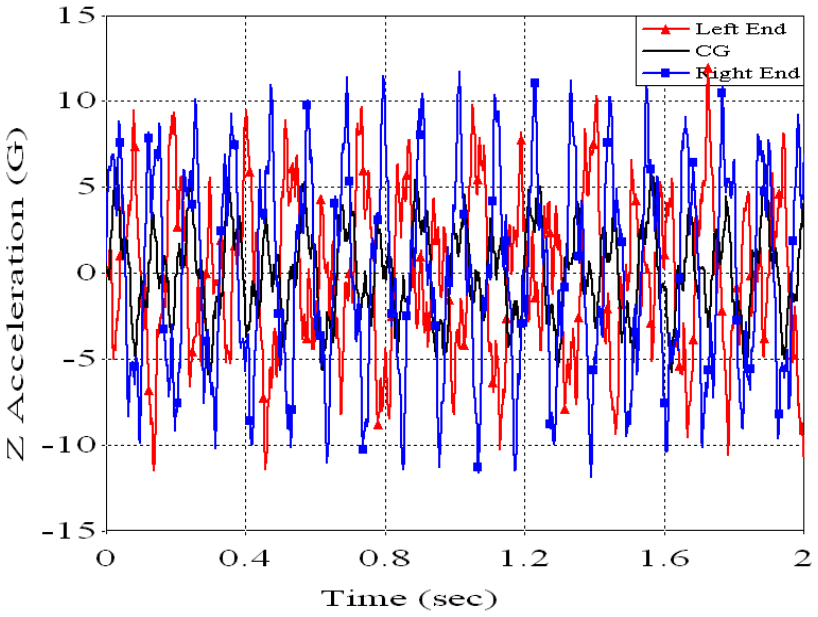

Figure 33. Time Histories for Z Acceleration at Various Locations

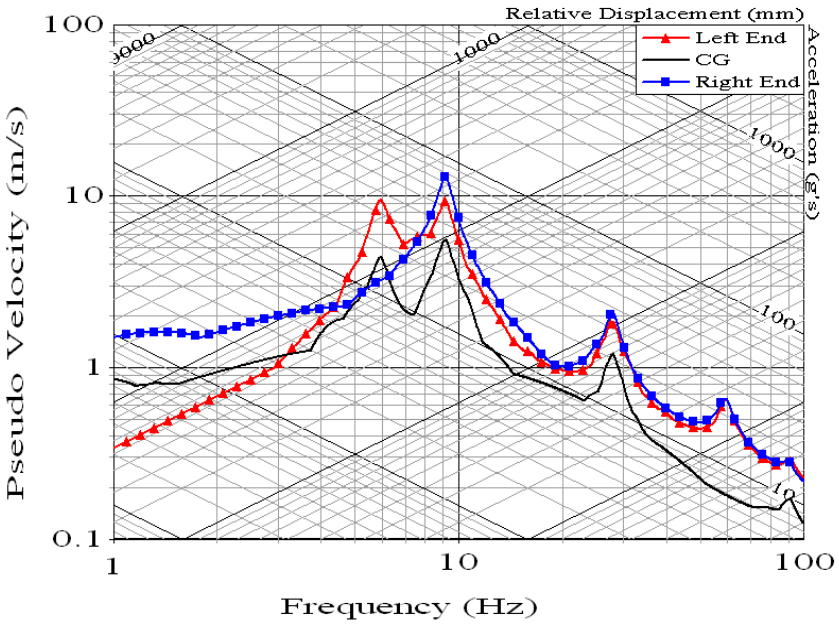

Figure 34. Pseudo Velocity for Z Acceleration at Various Locations

Figure 35 shows the vertical displacement (Z) of the isolators. The displacement at the right end is greater than that of the left end because the rotation drop is performed at the right position. Maximum vertical displacement (Z) of right isolator is 22.4mm, 16.2mm in the left isolator and only 9.4mm in the longitudinal isolator (Y).

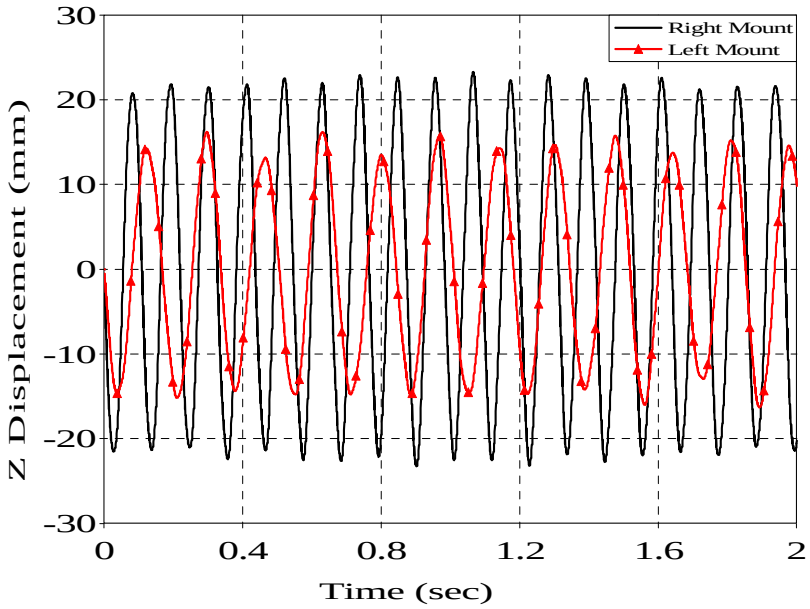

Figure 35. Displacement of a Shock Mount

C. NON-LINEAR TRANSIENT ANALYSIS

The shock mounts using rubber materials are typically found in container systems for large payloads like missiles. Generally rubber in compression exhibits nonlinear behavior with a hardening characteristic such that the stiffness increases with increasing deflection. For the small deflections the linear and hardening springs may be characterized in a similar fashion. But for the large deflection spring such as large container their behaviors are different. So it is important that the nonlinear characteristic is considered in the analysis of the packaging system that large deflection is occurred [Ref. 7, 8].

In this study, the effect of nonlinearity of the shock mount has been investigated using the nonlinear spring element as shown in Figure 36. Stiffness increases if the displacement of isolator is greater than 10mm. The analysis was performed using the MSC/NASTRAN Nonlinear transient module.

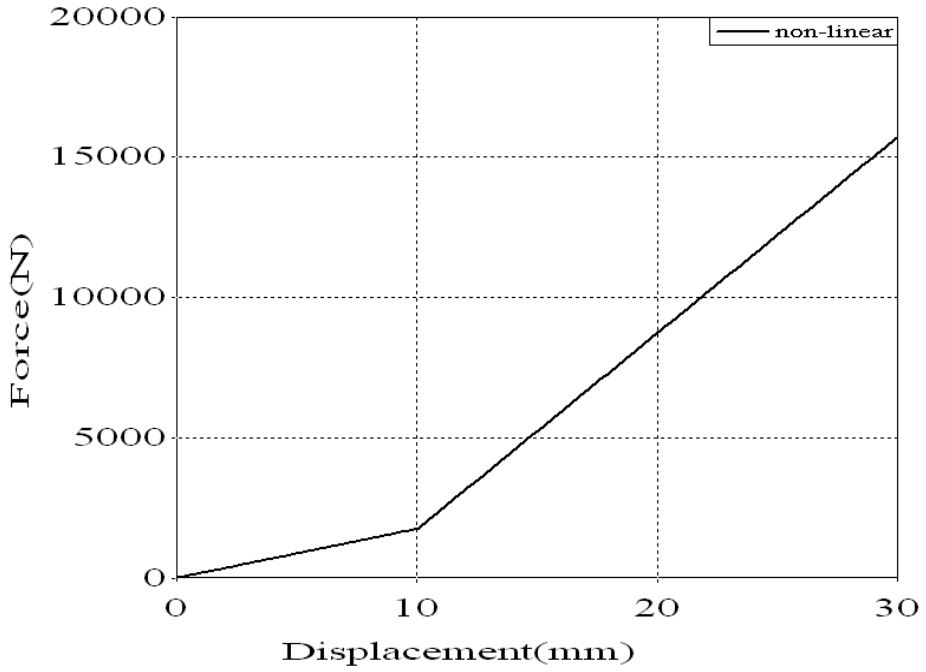

Figure 36. Non-linear Stiffness Curve

Figure 37 shows the displacement of the isolator for the nonlinear model compared to the results for the linear model. The displacement decreases in the nonlinear model.

Figure 38 shows the time history of the payload at the center of gravity. The acceleration level of the payload increased greatly in the nonlinear model.

Figure 39 shows the SRS of the payload at the center of gravity. In this figure, the response of the rigid body mode has changed from point *a* (9.17Hz, 32g) into point *a'* (11.2Hz, 40g) and the response of the first bending mode has changed from point *b* (27.9Hz, 21g) into point *b'* (29.4Hz, 90g). The change in the acceleration of the bending mode is greater than that of the rigid body mode. It shows that the nonlinearity should be considered when the packaging system for this type of long and flexible payload is designed.

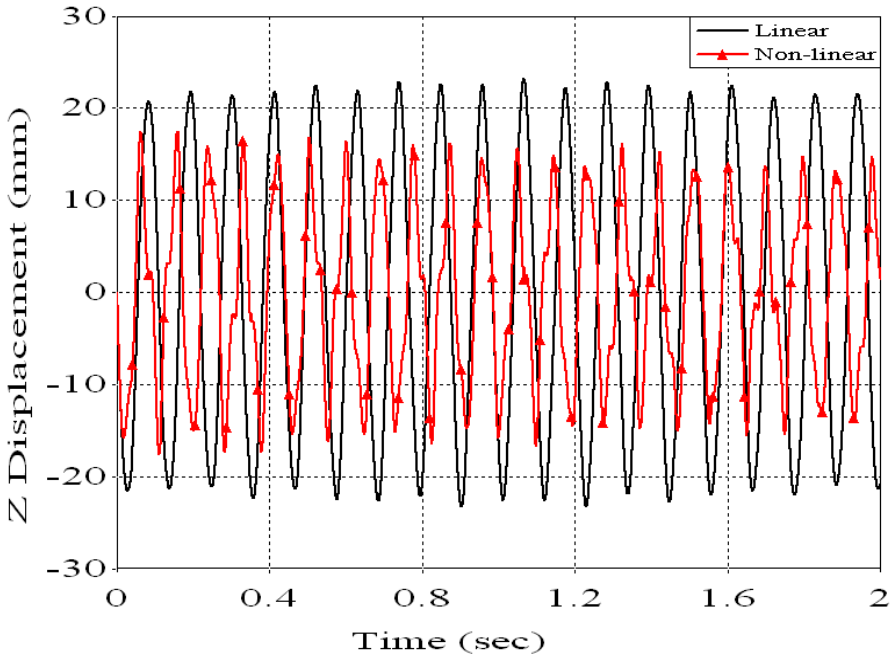

Figure 37. Displacement of Non-linear Shock Mounts

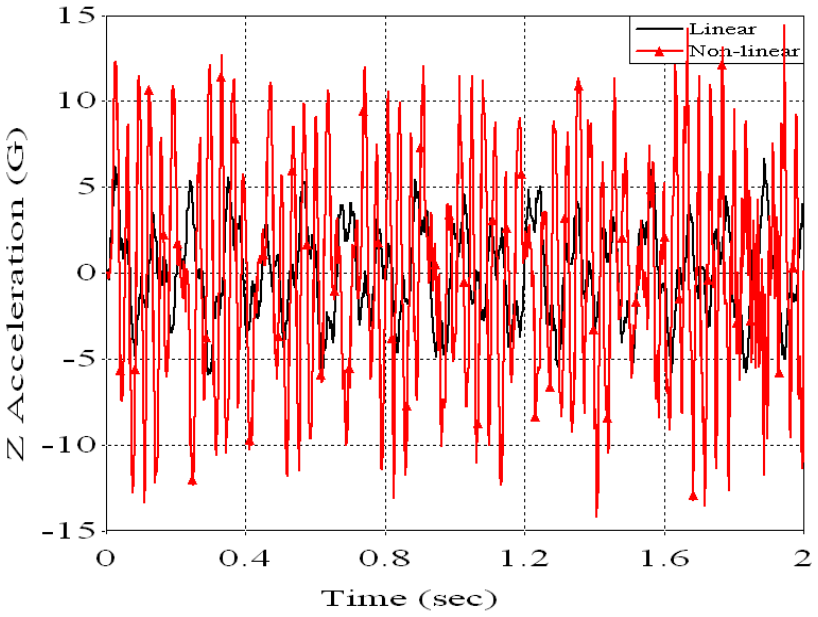

Figure 38. Time Histories for Z Acceleration of the Non-linear Stiffness

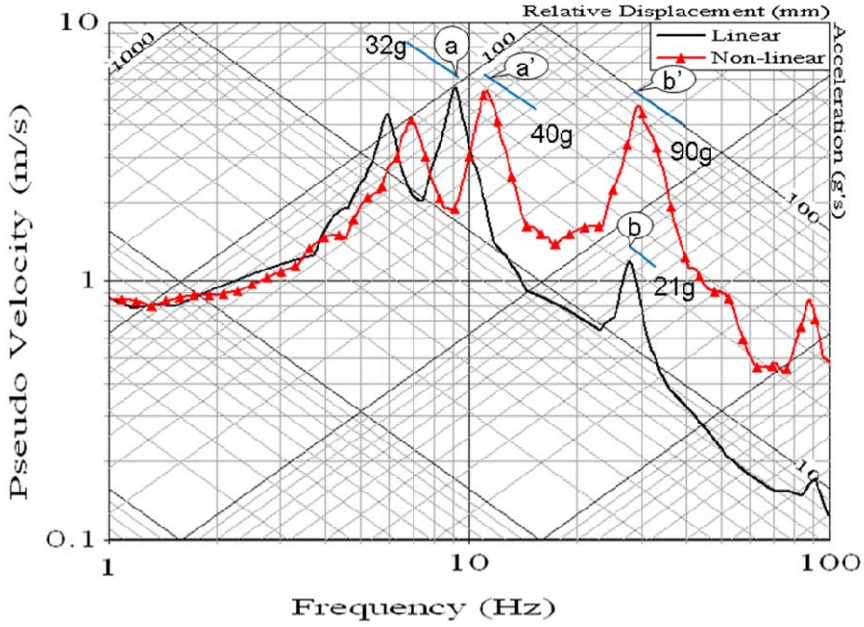

Figure 39. Pseudo Velocity for Z Acceleration of the Non-linear Stiffness

D. COMPARISON BETWEEN RESPONSES AND SPECIFICATION

The acceleration of the center of gravity of the payload is compared with the shock test specification, MIL-STD-810. The terminal peak saw tooth shock pulse shown in Figure 4 is recommended for use in the testing. The peak acceleration magnitude of the saw tooth pulse is 20g and its duration is 11ms, as is used in flight vehicle equipment testing.

Figure 40 shows the comparison of the pseudo velocity of the payload with the shock test specifications. The response in Z direction is higher than the one in Y direction. Both of the responses are higher than the specification standards in the low frequency range. As shown in the figure, the ranges that the responses exceed the specification are below 6.1Hz in Y direction and below 14.1Hz and between 26.3Hz and 29.8Hz in Z direction. It should be further investigated if there are natural frequencies of the equipment that fall in the frequency range that the responses exceed the specification.

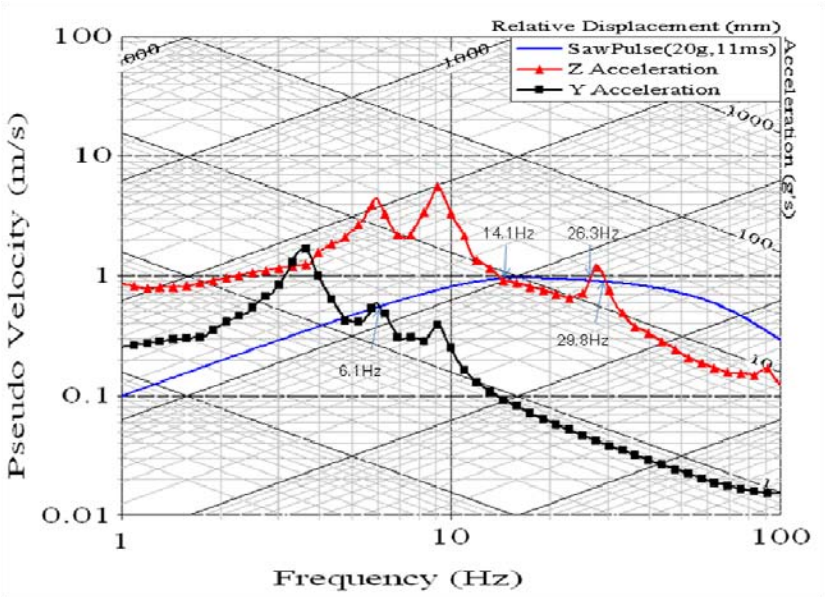

Figure 40. Comparison of SRS Responses and Specification

Figure 41 and 42 shows the specifications that cover all responses in the Y, Z direction respectively. As shown in these figures, the specifications of the saw tooth shock pulse that cover all responses in Y direction is 10g, 40ms and 80g, 55ms in Z direction.

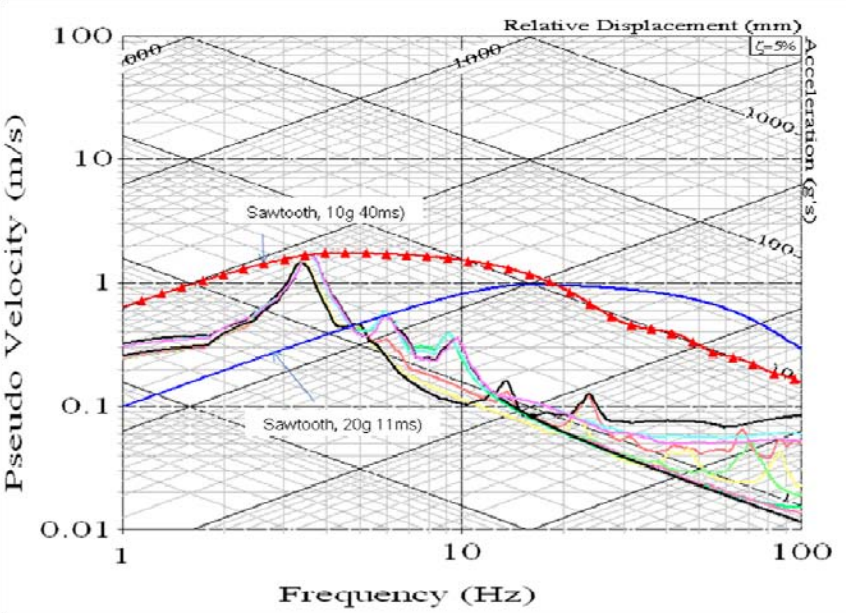

Figure 41. Comparison of All Y Accelerations with Specification

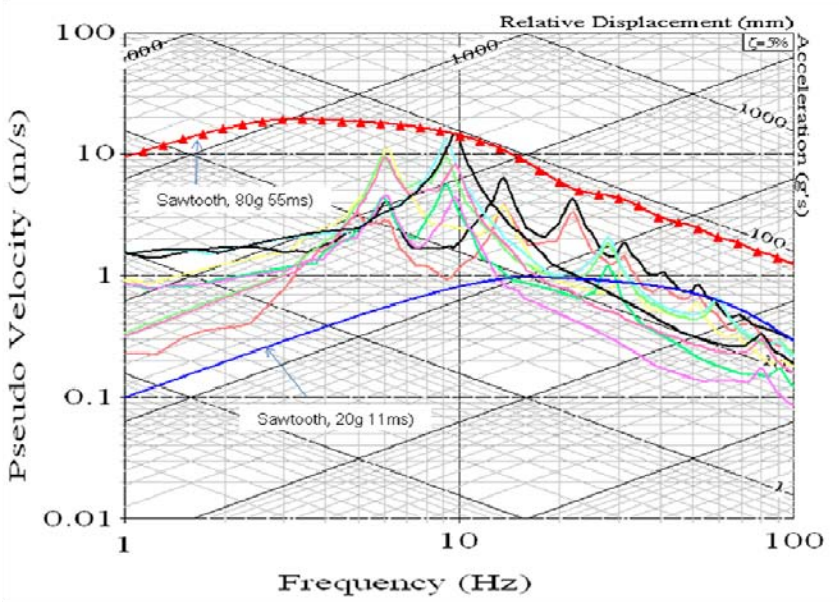

Figure 42. Comparison of All Z Accelerations with Specification

V. CONCLUSION

Damage Boundary Theory and Shock Response Spectrum Analysis have been investigated to evaluate the shock fragility of equipment. Computer simulation using MSC/NASTRAN have been performed to illustrate the shock design procedure of a packaging system. It is necessary that establish the shock fragility of equipment and design the shock isolation system to mitigate the shock environment loading upon the equipment. The Damage Boundary Test is an effective method in establishing the shock fragility level of the equipment itself, while the Shock Response Spectrum Analysis is useful in understanding the isolation level of packaging system.

The finite element modeling and subsequent computer simulations conducted for the rotational drop model have shown the effects of flexibility of the payload and the nonlinearity of the isolator. The results show that the close natural frequency between the rigid body mode of isolator and the bending mode of payload can increase the shock response of the payload. Furthermore, due to the nonlinearity of the isolator, the stiffness of isolator increases with increasing deflection, so the acceleration increases while the displacement of isolator decreases.

The results of simulation for the rotational drop have been compared with shock test specification, MIL-STD-810. The results of the simulation were found to be higher than the specification in the low frequency range.

THIS PAGE INTENTIONALLY LEFT BLANK

LIST OF REFERENCES

1. R. D. Kelly and G. Richman, “Principles and Techniques of Shock Data Analysis”, The Shock and Vibration Information Center, 1969.

2. Signalysis.com, “Shock Response Spectrum Analysis”

3. American National Standard Institute, Inc., “Shock Test Requirements for Equipment in a Rugged Shock Environment”, 2007.

4. Robert E. Newton, “Fragility Assessment Theory and Test Procedure”, Monterey Research Laboratory, Inc., 1968.

5. MIL-STD-810G Method 516.6, “Shock” in Environmental Engineering Considerations and Laboratory Tests, 2008.

6. ASTM D 3332-99, “Standard Test Methods for Mechanical-Shock Fragility of Products, Using Shock Machines”, ASTM International, 2004.

7. Herbert H. Schueneman, “Fragility Assessment: An In-Depth Look at A Now Familiar Process”, Westpak, Inc.

8. Herbert H. Schueneman, “Product Fragility Analysis Made Easy”, Westpak, Inc.

9. H. Himelblau and S. Rubin, “Vibration of a Resiliently Supported Rigid Body”, in Shock and Vibration Handbook, 4th ed., McGraw-Hill, 1996

10. Michael A. Talley and Shahram Sarkani, “A New Simulation Method Providing Shock Mount Selection Assurance”, Shock and Vibration 10, 2003, pp.231-267.

11. C. M. Harris, “Shock and Vibration Handbook, 4th ed”, McGraw-Hill, 1996

12. D. H. Merkle, M. A. Rochefort and C. Y. Tuan, “Equipment Shock Tolerance”, AD-A279689, Engineering Research Division of Air Force Civil Engineering Support Agency, 1993.

13. MSC Software Corporation, “MSC/PATRAN User’s Manual”, Los Angeles, CA, 2008

14. MSC Software Corporation, “MSC/NASTRAN User’s Manual”, Los Angeles, CA, 2008

THIS PAGE INTENTIONALLY LEFT BLANK

INITIAL DISTRIBUTION LIST

1. Defense Technical Information Center
   Ft. Belvoir, Virginia

2. Dudley Knox Library
   Naval Postgraduate School
   Monterey, California

3. Naval/Mechanical Engineering Curriculum Code 73
   Naval Postgraduate School
   Monterey, California

4. Visiting Professor Beomsoo Lim
   Department of Mechanical And Astronautical Engineering
   Naval Postgraduate School
   Monterey, California

5. Research Assistant Professor Jarema M. Didoszak
   Department of Mechanical and Astronautical Engineering
   Naval Postgraduate School
   Monterey, California

6. Distinguished Professor Emeritus Young S. Shin
   Department of Mechanical and Astronautical Engineering
   Naval Postgraduate School
   Monterey, California

7. Professor Young W. Kwon
   Department of Mechanical and Astronautical Engineering
   Naval Postgraduate School
   Monterey, California